Hydrological model skills change with drought severity; insights from multi-variable evaluation

Giulia Bruno[1,*], Francesco Avanzi[2], Lorenzo Alfieri[2], Andrea Libertino[2], Simone Gabellani[2], and Doris Duethmann[1]

[1] *Leibniz Institute of Freshwater Ecology and Inland Fisheries (IGB), Berlin, 12587, Germany*

[2] *CIMA Research Foundation, Savona, 17100, Italy*

[*] *Correspondence: giulia.bruno@igb-berlin.de*

Abstract

Hydrological models often do not properly simulate streamflow (Q) during extreme events, including droughts. Limited abilities in simulating Q during droughts may arise from a misrepresentation of Q generating processes during these periods, but little research has focused on distributed, process-based models over human-affected areas and extreme events. To shed more light into model consistency during these periods, we evaluated the ability of the hydrological model Continuum in simulating Q over the human-affected Po river basin in Italy during droughts of different severity over the last 13 years, including the severe 2022 event. To investigate the causes for potential model deterioration during severe droughts, we assessed the simulation of evapotranspiration (ET) and Terrestrial Water Storage (TWS) against independent remote sensing-based benchmarks, and possible inconsistencies in forcing and benchmark data. Finally, we included a moderate drought in the calibration period, as potential strategy to improve model performances during severe droughts. The model represented well Q (KGE = 0.81 for the outlet of the basin), ET (r = 0.94) and TWS (r = 0.76) over the whole study period. Focusing on Q and specific sub-periods, model performances were comparable during wet years (2014 and 2020) and moderate droughts (2012 and 2017), with KGE across the 38 study sub-catchments of 0.59±0.32 (mean ± standard deviation) during wet years and 0.55±0.25 during moderate droughts. The model simulated Q well for the outlet section of the basin also during the severe 2022 drought (KGE = 0.82). However, performances across the sub-catchments declined in 2022 (KGE = 0.18±0.69). For the severe drought, we detected a decrease in model performances for ET, in particular over human-affected croplands (mean decrease in r by 105% and mean increase in nRMSE by 86%). Furthermore, calibrating during a moderate drought did not improve model performances in 2022 (KGE = 0.18±0.63), pointing to the fairly unique conditions of this period in terms of hydrological processes and human interference on them. Our study highlighted decreased model skills specifically during a severe drought and identified the neglection of irrigation as the most plausible cause for this. Given projected increases in severe droughts and the frequent modelling simplification of human activities, despite their heavy interference in many regions, our findings are highly relevant to move towards more robust hydrological modelling in a changing climate and the Anthropogenic era, to support management and adaptation strategies.

Keywords

hydrological modelling; droughts; human-water interactions; irrigation; evapotranspiration; storage

1 Introduction

Droughts propagate from precipitation deficits (meteorological droughts) to streamflow deficits (streamflow droughts), by affecting all components of hydrological systems [1], and resulting in severe and multifaceted impacts on the environment, societies, and economies [2]. The frequency, severity, and duration of streamflow droughts will likely increase in a warming climate, with increasing impacts as well [3]. Therefore, robust modelling of water availability throughout the whole hydrological cycle during droughts is essential today to inform water management, disaster risk reduction, and climate change adaptation strategies.

Distributed process-based hydrological models allow spatial estimates of hydrological fluxes and states [4], even at large scales and hyper-resolutions (< 1 km [5]). Climate impact assessments [6, 7, 8], drought monitoring [9, 10, 11] and forecasting systems [12, 13, 14], and drought studies in general [15, 16, 17] widely use these models today. Yet, some studies revealed poor model performances when simulating streamflow droughts [18] and their generating processes [19]. Furthermore, human activities heavily modify the hydrological cycle [20] and streamflow droughts [21] at present, but their representation in hydrological models remains challenging [22].

Many hydrological models show decreases in streamflow (Q) performance during climatic conditions that differ from those of the calibration period [23, 24, 25] and this poses challenges during particularly severe droughts [26]. While some studies demonstrated the ability of distributed process-based hydrological models in reproducing dry conditions [27, 16], research on their robustness during severe droughts is still limited.

Previous studies revealed that decreased model performances in Q simulation during severe droughts may be related to poor simulation of actual evapotranspiration (ET, [28]) or Terrestrial Water Storage (TWS, i.e., in the groundwater, soil moisture, surface water bodies, snow, and ice storages, [29, 30]). For instance, [28] showed that a semi-distributed hydrological model had statistically significant decreases in Q

and ET simulation during the 2012–2016 drought over a Californian river basin, but not in the simulation of subsurface storage; thus, they argued that the misrepresentation of ET, and its climate elasticity in particular, drove the deterioration in Q modelling skills. [30] found that in Australian catchments where common lumped conceptual models simulated Q poorly during the Millennium drought, the models also failed in reproducing long-term decline in storage. This indicates that evaluating hydrological models against multiple hydrological fluxes and states represents a way to analyze causes of poor model performances and hence move towards more robust modelling [31]. ET and TWS remote sensing-based products can be particularly useful for distributed model evaluation [32, 33] as they allow to check also the spatial representativeness of models. Nonetheless, model evaluations during severe droughts using spatially distributed ET and TWS remote sensing-based products is still rare in the literature.

Finally, some studies suggested that including dry periods in the calibration can improve Q simulation during droughts [24, 16], but the validity of this for severe droughts beyond the calibration conditions still remains open [28].

To contribute to filling these knowledge gaps, we aimed to answer three research questions: (i) does Q simulation performance deteriorate with increasing drought severity for a distributed process-based hydrological model?; (ii) if so, what are the causes for the decrease in Q simulation performance during severe droughts?; (iii) does including a moderate drought in the calibration period improve model skills during severe droughts?

For this purpose, we analyzed the performance of the hydrological model Continuum [34] over the Po river basin in northern Italy during the flood- and drought-rich period September 2009–August 2022. We calibrated the model against Q data and evaluated the model capability in reproducing the spatio-temporal variability of Q, ET, and TWS for the entire basin and 38 sub-catchments, during wet years and droughts of varying severity, by using independent ground- and remote sensing-based benchmarks.

2 Data and methods

2.1 Study area

For this study, we selected the Po river basin, as a drought-prone area [35, 36, 37, 38], and major catchment in Italy for drainage area (around 74000 km^2) and socio-economic relevance with 27% of Italian population, 35% of agricultural production, and 37% of industrial production [39].

The Po river basin lies in northern Italy and part of the Swiss Canton Ticino region (Figure 1). The Alps border the basin in the west and north, and the Apennines in the south, while the Po plain characterize its central part. Consequently, the basin shows a steep orographic gradient and elevations range from sea level to about 4800 m above sea level [40] (Figure 1a).

The climate in the area transitions from alpine and cold, with a bimodal annual precipitation cycle and peaks in autumn and spring, to temperate with a dry season and most of the precipitation (P) in winter [41, 42] (Figure 1b). Snow contribution to streamflow (Q) is relevant especially at high elevations in the northern and western part of the basin, where the mean annual ratio between peak snow water equivalent and annual Q can exceed 60% [43]. Subsequently, Q has usually two peaks, one in autumn for heavy rainfall events and one in spring for rainfall events and snowmelt, and a low-flow period during summer.

As a result of topographic and climatic characteristics, a variety of land cover types characterize the basin (Figure 1c): transitions between bare soil, grassland, and forests following the elevational gradient in the mountainous parts, shrubland in the temperate and dry areas in the southwestern part, and cultivated and urban areas in the central lowlands [44]. In addition to three major lakes, around 180 multi-purpose reservoirs alter the flow in the basin [39]. Anthropogenic water withdrawals for irrigation, industrial, and drinking water uses from surface- and ground-water further affect the hydrological cycle in the area. Irrigation accounts the most among the water uses (60%), responsible for water withdrawals of around 17*10^9 $m^3 year^{-1}$ (i.e., 5% of mean annual precipitation), mainly from surface water and with further increases by up to 15% during droughts [39].

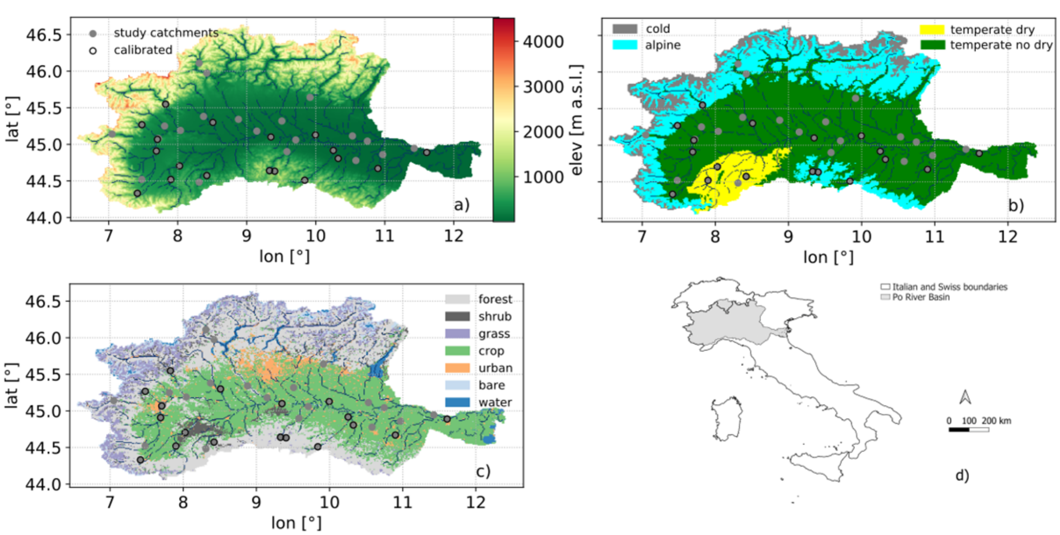

Figure 1: Overview of the study area: maps with (a) elevation, (b) climate, (c) land cover types, and (d) location of the model domain, modelled river network (dark blue line), and study sub-catchments outlets (grey dots, with black edge if used in model calibration, Section 2.4.2). For data sources please refer to Table S1.

2.2 Hydrological modelling

The hydrological model Continuum [34] is an open-source continuous and grid-based hydrological model (https://github.com/c-hydro). It simulates the main hydrological processes in a process-oriented but parsimonious way, by solving the mass and energy balances with up to 8 calibration parameters [34, 45, 46]. The model also includes optional modules to simulate flow regulation by natural and man-made reservoirs, and other hydraulic infrastructures (water withdrawals and releases), with additional parameters to this end. Continuum does not explicitly represent irrigation fluxes currently.

Here we set up the model to simulate snow accumulation and melting, vegetation interception, energy fluxes and evapotranspiration (ET), subsurface water dynamics, major reservoirs, and surface flow routing [47]. In Figure S1 we provided a scheme of the model configuration, along with model fluxes and states. The snow accumulation and melting module relies on mass conservation and a hybrid approach for snowmelt, which couples a radiative term with a temperature-driven one [45]. Vegetation interception is simulated through an empirical equation, [34] and references therein. The dynamics of water in the soil is modelled through an adaptation of the Horton equation and in the groundwater by a modification of the Darcy law, [34] and references therein. The surface flow routing scheme is based on a Manning-type equation [46]. We refer the reader to [34] for details on the model, [45] on its snow module, and [46] on the surface flow routing scheme.

In this work, we run Continuum on a regular grid at 0.009° resolution (for a total of 212901 grid cells) and 1 hour time step [47] over the hydrological years 2009–2022, with the first year as warm-up period. Please note that throughout the manuscript we referred to hydrological years, spanning from August to September, rather than calendar years.

2.3 Data

2.3.1 Model input data

In this work, we used the same model setup as [47], to which we refer for details on the input datasets required by the model (Table S1).

As forcing data, we used P maps from the Modified Conditional Merging (MCM) algorithm [48]. Over the study area, MCM blends data from 1377 P gauges and radars from the Italian Civil Protection Department (DPC) [47], and outperformed gauge-only [48] and satellite products [47]. For the other meteorological variables required by the model (air temperature, relative humidity, wind speed, and shortwave solar radiation), we used maps interpolated from ground-based data provided by DPC [47].

We further used information from DPC and a global product for dams [49] to derive the parameters required for the representation of reservoirs in the model (Section 2.2).

2.3.2 Data for model calibration and evaluation

For model calibration and evaluation, we exploited a set of independent ground- and remote sensing-based datasets (Table S1). For Q, we used quality-checked daily mean Q time series for 38 sub-catchments in the Po river basin (Figure 1) from DPC and Italian regional hydrometeorological offices [47, 50]. We selected the study sub-catchments according to data availability (maximum 6 months of missing data). These sub-catchments reflect the variety of topographic, climatic, and land cover characteristics in the study area (Table S2).

For ET, we applied the METv2 product by the Land Surface Analysis of the EUMETSAT Satellite Application Facility (LSASAF) [51, 52]. The LSASAF product provides gridded ET estimates by exploiting data from the Meteosat Second Generation satellite at a spatial resolution of 3.1 km at the sub-satellite point and at a temporal resolution of 1 hour. It derives ET estimates from a surface energy model, based on the Soil-Vegetation-Atmosphere-Transfer scheme described in [51], and remote-sensed data. We chose this product since it showed reasonable agreement with alternative gridded ET products and eddy-covariance data over Italy during droughts [50]. We used the LSASAF product as benchmark of simulated ET for catchment- and regional-scale analyses (Section 2.4.3), by retaining only those days with more than 75% of hourly data available.

Finally, we employed TWS data from the Gravity Recovery And Climate Experiment (GRACE) and GRACE Follow-On (GRACE-FO) missions, henceforth GRACE data. GRACE launch was in April 2002 and its dismissal in June 2017, whereas GRACE-FO is operational since May 2018. These missions consist of two twin satellites measuring variations in distance between them and, thus, in the Earth's gravity field. Consequently, GRACE data provide estimates of changes in mass over a certain area from which variations in TWS can be derived. As GRACE data, we used the recently developed mass concentration (MASCON) solution, as it is particularly suited for hydrological applications compared to the traditional spherical harmonics solution [53]. MASCON does not require any significant postprocessing, while minimizing errors due to the leakage of the signal from land to oceans. We processed the latest products of GRACE MASCONS (release 06) from the Center for Space Research at the University of Texas (CSR) [54, 55], the NASA Jet Propulsion Laboratory (JPL) [56, 57], and the NASA Geodesy and Geophysics Research Laboratory (GSFC) [58] at monthly temporal resolution, and spatial resolutions of 1° for CSR and GSFC products and 0.5° for the JPL product. We regridded, using a nearest neighbour approach, the three products to a common grid of 0.5° spatial resolution. Then, we considered the mean among them to reduce the uncertainties associated with specific GRACE products [59]. GRACE data provide anomalies regarding the period 2004–2009, therefore we converted them to anomalies over the study period by subtracting their long-term means [59]. Due to the coarse spatial resolution of GRACE data and the relatively small drainage area for most of the study sub-catchments (Table S2), we used GRACE data only for a catchment-scale analysis at the outlet section of the basin (drainage area = 72545 km^2).

2.3.3 Potential data inconsistencies

Inconsistencies in the data used to force and evaluate the model can affect the outcomes of model evaluations [32]. We quantified these potential inconsistencies at annual scale through the observed water imbalance (P-Q-ET-TWSC, with TWSC as change in TWS between the end and the beginning of the hydrological year).

2.4 Analyses

2.4.1 Experimental design

We performed two calibration-evaluation experiments (Table 1) to study (i) model performances over varying wetness conditions and (ii) whether including a moderate drought improved model robustness to severe droughts. For each calibration experiment, we evaluated model performances during the whole study period and periods with contrasting climatic conditions.

We characterized the climatic conditions for the study sub-catchments in terms of their annual P standardized anomalies according to Equation 1:

$$P_{\mathrm{anom}}(t) = \frac{P(t) - \overline{P}}{\sigma_{\mathrm{P}}} \tag{1}$$

where $\overline{P}$ is the mean and σ_{P} the standard deviation of annual P over the study period. We defined wet (or dry) years as those years with positive (or negative) annual P standardized anomalies for most of the study sub-catchments (Figure S2). Further, we referred to dry years as droughts, and we defined them as moderate or severe in terms of decreasing annual P standardized anomalies (Table 1).

We first calibrated the model during the years 2018 and 2019 which represented average conditions regarding annual P (calibration 1), and we evaluated model performances over the whole study period, the wet years 2014 and 2020, the moderate droughts 2012 and 2017, and the severe drought 2022 (Sections 3.2 and 3.3). Then, we calibrated the model during a moderate drought (calibration 2, over the years 2016 and 2017) and we repeated the model evaluation, with particular focus on the severe drought (Section 3.4).

Table 1: Calibration and evaluation periods, and their climatic characteristics in terms of annual P standardized anomalies across the study sub-catchments (mean $\pm$ standard deviation). Years reported here refer to hydrological years rather than calendar years. For the evaluation over the whole study period, we reported averages annual anomalies across the study sub-catchments.

Purpose	Climatic conditions	Period	Annual P standardized anomalies [-]
Calibration 1	average conditions	2018; 2019	-0.11±0.52; 0.34±0.42
Calibration 2	including a moderate drought	2016; 2017	-0.56±0.31; -0.85±0.61
Evaluation	wet years	2014; 2020	1.14±0.6; 1.48±0.34
Evaluation	moderate droughts	2012; 2017	-0.8±0.39; -0.85±0.61
Evaluation	severe drought	2022	-1.68±0.43
Evaluation	whole study period	2010–2022	1.02e-16±0.46

2.4.2 Model calibration

We deployed a multi-site calibration procedure to calibrate the model against Q data, following [47] for the calibration approach and the selection of calibration sub-catchments (18 sub-catchments, dots with black edges in Figure 1). For calibration, we used 2-year periods, with the first 6 months for model warm-up and the remaining 1.5 years for calculating model performances. We did not choose a longer calibration period due to computational reasons, in agreement with previous works using the same model [48, 47] and distributed models [60]. We calibrated four model parameters (Figure S1 and Table S3): the Curve Number (CN), the field capacity (c_{t}), the infiltration velocity at saturation (c_{f}), and a parameter regulating the baseflow from the groundwater storage (w_{s}). CN, c_{t}, and c_{f} are spatially distributed parameters, while w_{s} is lumped for the whole model domain. We set the first guess parameters from (i) global maps of soil characteristics [61] and land cover [44] for CN, c_{t}, and c_{f}, and (ii) expert knowledge for w_{s} (Table S3 and Figure S3). We then used an iterative parallel search algorithm [47] to optimize scaling factors for these first guess parameters. This procedure allowed to preserve the spatial patterns of the first guess parameters while minimizing a cost function. To this end, the algorithm iteratively explores the parameter space with a Gaussian Latin hypercube sampling strategy [62] and uses the point which minimizes the cost function at each iteration as center for the subsequent sampling. Here we set $N = 50$ as number of samples (i.e., model runs) at the first iteration and then reduced this number by 20% at each iteration for computational efficiency. We further set the convergence of the algorithm as an improvement <1% in the cost function compared to the previous iteration. We based the cost function on a sum of Kling-Gupta Efficiency (KGE [63]) on the daily Q of each calibration sub-catchment, weighted with the logarithm of the sub-catchment area, to give more emphasis to the downstream sub-catchments [47]. The KGE is an aggregated measure of the agreement in timing, magnitude, and variability between simulations and observations (Equation 2):

$$\mathrm{KGE} = 1 - \sqrt{(r-1)^2 + (\beta-1)^2 + (\gamma-1)^2} \tag{2}$$

where r is the Pearson's correlation coefficient (timing component), β is the ratio between simulated and observed means (bias component), and γ is the ratio between simulated and observed coefficients of variation (variability component). KGE has an optimal value = 1, for each component as well, and no-skill threshold over mean flow as predictor at -0.41 [64]. We used the KGE, instead of other metrics tailored specifically to low-flows [65] for instance, because we intended to evaluate a model set up for general hydrological applications, such as climate impact assessments, and not to optimize the low flows at the expense of other Q regimes. We reported the KGE from the two calibration experiments in Table S4.

2.4.3 Model evaluation

We evaluated model performances in reproducing the temporal variability of Q, catchment-average ET, and catchment-average TWS anomalies at monthly time scale, which is the temporal resolution of GRACE data. To evaluate model skills for TWS, we reconstructed the simulated states in model storages, i.e., from the water volumes in the snow, vegetation, surface water, soil, and groundwater storages (Figure S1). We then computed the TWS anomalies by subtracting the long-term mean for the simulation period. Additionally, we evaluated where deviations between the model and the remote sensing-based ET product locate in a regional-scale analysis, by computing pixel-wise deviations on normalized fluxes. Since ET and TWS are highly seasonal, we indeed evaluated model capability in simulating their seasonality (i.e., monthly mean values) and deviations from it (i.e., monthly standardized anomalies) [32]. We computed the monthly standardized anomalies (z_{anom}) as the anomalies relative to the monthly climatology (Equation 3):

$$z_{\mathrm{anom}}(t_i) = \frac{z(t_{\mathrm{i}}) - \overline{z}_{\mathrm{i}}}{\sigma_{\mathrm{z_i}}} \tag{3}$$

where z is the value at each time step, $\overline{z}_{\mathrm{i}}$ and $\sigma_{\mathrm{z_i}}$ are the long-term mean and standard deviation for month i.

We evaluated the model capability in simulating long-term changes as well, even though only in a qualitative way, through 24-month means, since we considered the study period too short for trend detection.

As performance metrics, we used the KGE and its components (Section 2.4.2) for Q, and the Pearson's correlation coefficient (r, with $r \in$ [-1, 1] and 1 as optimal value) and the normalized Root Mean Square Error (nRMSE) for ET and TWS standardized anomalies. We computed nRMSE according to Equation 4:

$$\mathrm{nRMSE} = \frac{\sqrt{\frac{1}{N}\sum_{i=1}^{N}(X_{\mathrm{sim,i}} - X_{\mathrm{obs,i}})^2}}{\sigma_{\mathrm{X_{obs}}}} \tag{4}$$

where $X_{\mathrm{sim,i}}$ is the simulated variable at time step i, $X_{\mathrm{obs,i}}$ the observed, $\sigma_{\mathrm{X_{obs}}}$ the observed standard deviation, and N the number of time steps, leading to nRMSE $\in [0, +\infty)$ and 0 as optimal value [66]. We normalized the RMSE to allow a fair comparison among sub-catchments/grid cells that may have different observed ranges. For normalizations, we used the standard deviation rather than the mean to avoid numerical issues when the latter is close to zero, as it is often the case for TWS anomalies.

To identify statistically significant differences across the evaluation periods, we used a two-sample t-test for the mean across the study sub-catchments ($p < 0.01$).

3 Results

3.1 Hydroclimatological conditions during droughts

Three droughts occurred in the study area over 2010–2022, namely in 2012, 2017, and 2022 - which extended to 2023 [67] -, as depicted by annual P standardized anomalies (Table 1 and Figure S2) and reported by [35, 36, 37, 38]. Low winter P characterized the three events (Figure 2a). However, duration and severity of low P values differed among the events, with moderate annual P standardized anomalies in 2012 and 2017, and severe anomalies in 2022 (Table 1). During the three events, the meteorological drought propagated rather differently through the hydrological cycle (Figure 2). For 2012 and 2017, the LSASAF product showed higher-than-usual ET during spring (Figure 2b), but lower-than-usual ET during summer (integrated over the entire basin, August ET = 52 mm month^{-1} in 2012 and 46 mm month^{-1} in 2017 compared to a climatology of 71$\pm$15 mm month^{-1}, with climatology expressed as the mean $\pm$ standard deviation over the study period 2010–2022). On the contrary, the ET product showed higher-than-usual values during the 2022 drought (Figure 2b, July ET = 124 mm month^{-1} compared to a climatology of 87$\pm$18 mm month^{-1}). TWS was within the climatology in 2012 and 2017, whereas it was already low at the beginning of 2022 (Figure 2c, September TWS anomaly = -92 mm compared to a climatology of -58$\pm$37 mm) and during summer it reached the minimum value over the whole study period (August TWS anomaly = -158 mm compared to a climatology of -54$\pm$56 mm, Figure 2c). As a result, Q showed moderately low values throughout 2012 and 2017 (Figure 2d, July Q = 18 mm month^{-1} in 2012 and 25 mm month^{-1} in 2017, compared to a climatology of 30$\pm$13 mm month^{-1}), while it experienced lower-than-usual values during most of 2022 (July Q = 9 mm month^{-1}). In summary, hydroclimatic conditions during the 2022 drought were extraordinary for the study period, characterized by severe P deficits during most of the year, positive ET anomalies during summer, low TWS levels throughout the entire year, and consequently strong negative Q anomalies [68].

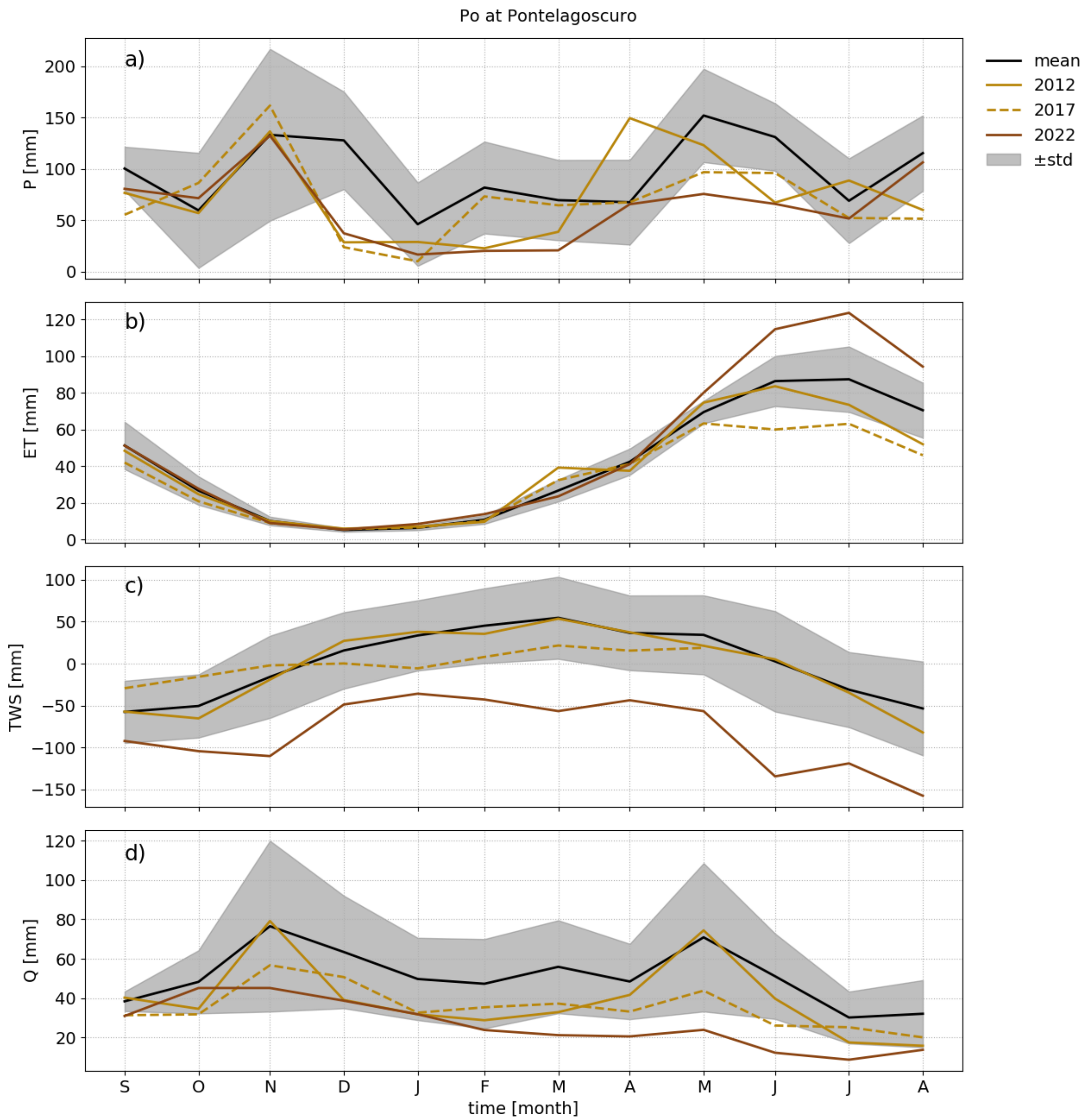

Figure 2: Hydroclimatic conditions during the study period: observed monthly climatology (mean ± standard deviations over 2010—–2022) and monthly values during drought years, for the basin outlet (Pontelagoscuto) for P (a), ET (b), TWS (c), and Q (d).

3.2 Model evaluation for streamflow during droughts of varying severity

Model performances for Q were comparable during wet years, moderate droughts (Figure 3a, b, and d), and the whole study period (Table S3) for the model calibrated during average climatic conditions (Section 2.4.2). Across the sub-catchments, mean KGE (± 1 standard deviation) was equal to 0.59(±0.32) during wet years, 0.55(±0.25) for moderate droughts, and 0.7(±0.19) over the whole study period. At the basin outlet Pontelagoscuro, the model represented properly the slight decline in Q since autumn 2019 and the low Q values during the severe 2022 drought (KGE = 0.82, Figure 4a).

Nonetheless, model performances across the study sub-catchments showed a decrease during the severe 2022 drought (KGE = 0.18±0.69, Figure 3c and d). Even though the model preserved some skill over the climatological mean [64], performances were low especially in the evaluation catchments and in terms of bias with a general overestimation of Q (Figure S4, β = 1.37±0.75). The other components of KGE (r and γ) did not change significantly between moderate droughts and the severe drought (Figures S5 and S6). Therefore, we investigated the simulation of ET and TWS, and potential inconsistencies in observed data as possible culprits for Q overestimation during 2022 (Section 3.3).

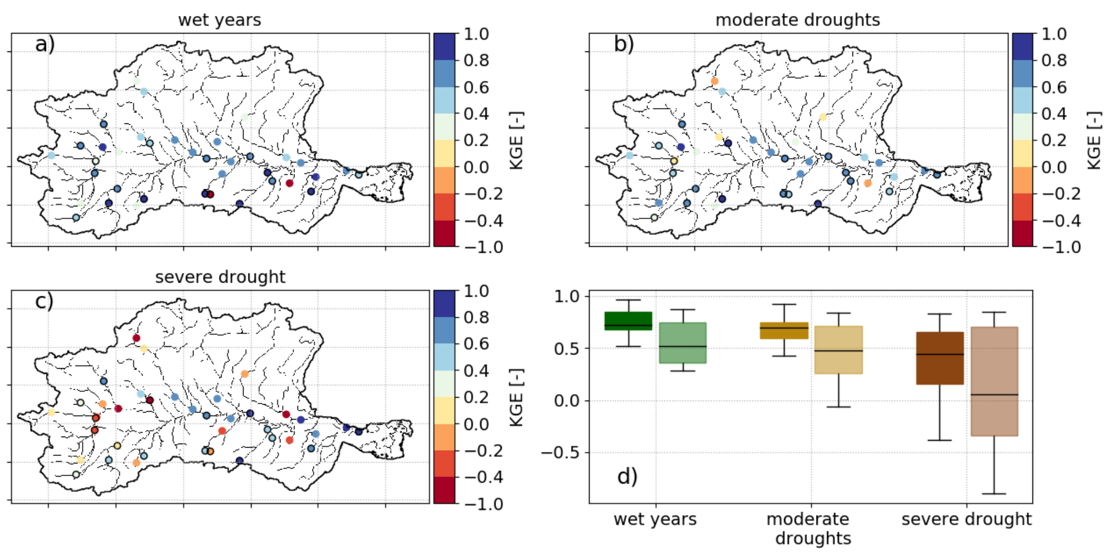

Figure 3: Streamflow (Q) model performances for the model calibrated during average climatic conditions (Section 2.4.1): KGE values on monthly Q during wet years (a), moderate droughts (b), and the severe drought (c) for each study sub-catchment, and their distributions as boxplots (d) grouped by calibration (full colours) and evaluation (light colours) sub-catchments.

3.3 Potential causes for streamflow overestimation during the severe drought

The model generally performed well for ET during the whole study period and moderate droughts, but less during the severe drought. Integrated over the entire basin, the model simulated properly both ET monthly values (r = 0.94 and nRMSE = 0.36 over the whole study period, Figure 4d) and seasonality (r = 0.99 and nRMSE = 0.18 for monthly mean ET, Figure 4e), although it overestimated slightly ET during winter and spring, and it simulated an earlier ET peak in summer (Figure 4e). The model performed less well in simulating ET deviations from seasonality, with r = 0.52 and nRMSE = 0.98 for monthly ET standardized anomalies over the whole study period (Figure 4f). Across the study sub-catchments, the simulation of monthly ET standardized anomalies was skillful during moderate droughts (mean r = 0.81 and mean nRMSE = 0.68, Figure 5a and d), but it deteriorated significantly during the severe drought (mean r = 0.05 and mean nRMSE = 1.61, Figure 5b and e). Performance decreases for monthly ET standardized anomalies during the severe drought were not uniform throughout the model domain (Figure 6b and e) and showed a clear pattern with land cover. Model deterioration was particularly strong for croplands, mostly located in the central part of the domain (Figure 1c), with mean r = 0.59 and mean nRMSE = 0.93 across the crop cells during moderate droughts, and mean r = -0.03 and mean nRMSE = 1.74 during the severe drought (Figure 6c and f).

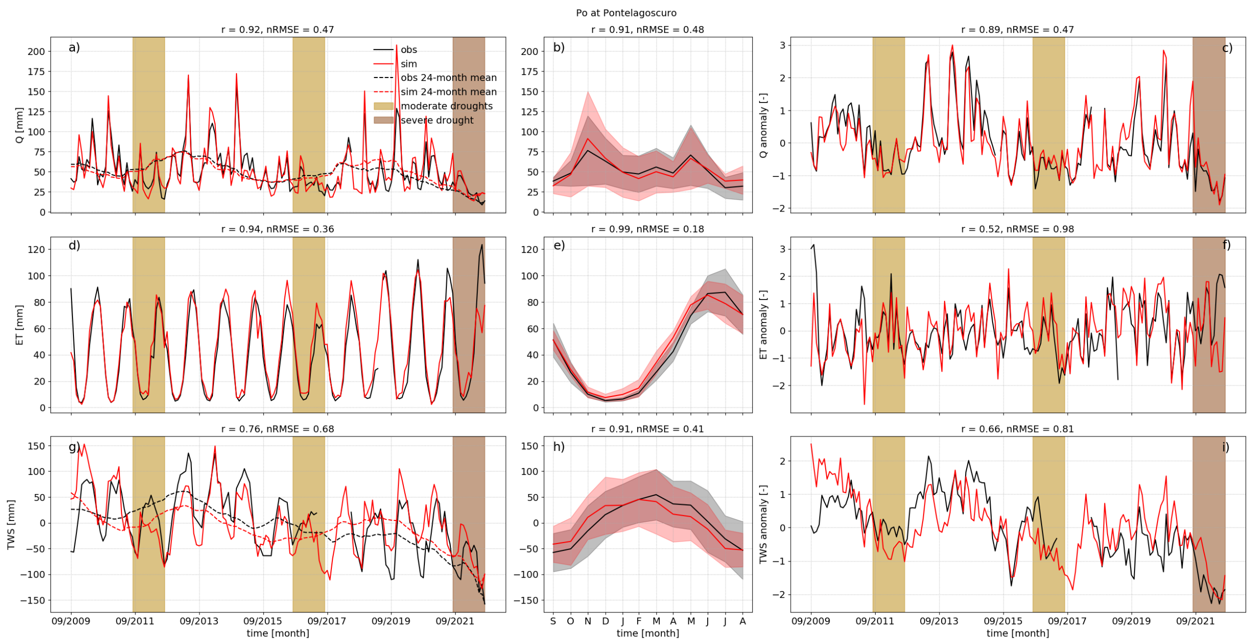

Figure 4: Model evaluation for catchment-average streamflow (Q), evapotranspiration (ET), and Terrestrial Water Storage (TWS) anomalies for the basin outlet (Pontelagoscuro): time series of benchmark (black) and simulated (red) Q (first row), ET (second row), and TWS (third row) monthly values and 24-month rolling means (first column), monthly means (second column), and monthly standardized anomalies (third column). Shading in panels (a), (c), (d), (f), (g), and (i) refers to moderate and severe droughts, while shading in panels (b), (e), and (h) corresponds to ± one standard deviation in monthly values.

Over the entire basin, the model represented well the decline in TWS over the recent years (Figure 4g), as well as TWS seasonality with the refilling of storage in autumn and winter, and its depletion in spring and summer (r = 0.91 and nRMSE = 0.41, Figure 4h). The model simulated properly the negative storage conditions in autumn 2021 (simulated TWS standardized anomaly = -0.66 and observed = -0.6 in September 2021, Figure 4g) and it overestimated slightly TWS during the depletion phase (simulated TWS standardized anomaly = -1.4 and observed = -1.9 in August 2022).

Potential inconsistencies in observed data, as quantified by the observed water imbalance, did not differ

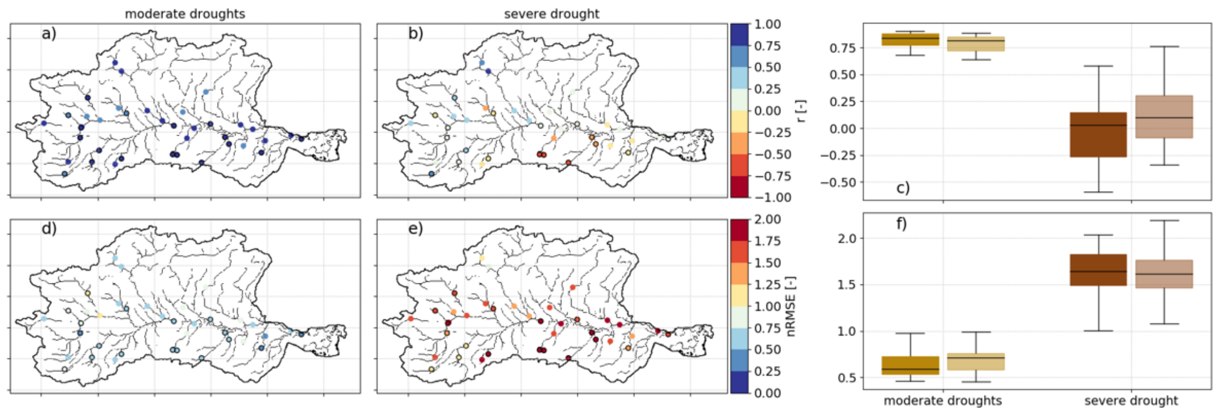

Figure 5: Model performances for the simulation of catchment-average evapotranspiration (ET): r and nRMSE on monthly ET standardized anomalies over moderate droughts (a and d) and the severe drought (b and e) for each study sub-catchment, and errors distributions as boxplots (c and f), grouped by calibration (full colours) and evaluation (light colours) sub-catchments.

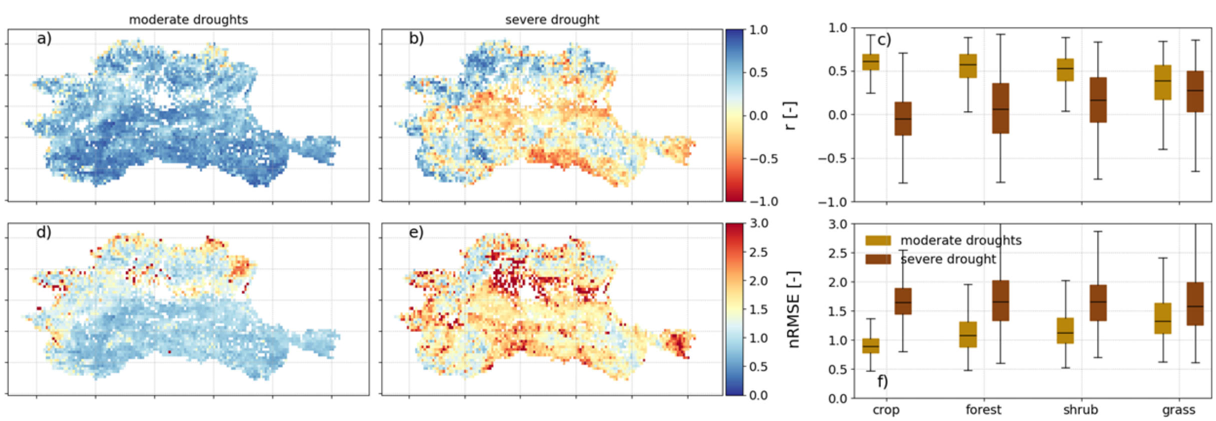

Figure 6: Spatially distributed model performance regarding the simulation of evapotranspiration (ET): maps of pixel-wise r and nRMSE on monthly ET standardized anomalies over moderate droughts (a and d) and the severe drought (b and e), and errors distributions as boxplots per each land cover type (c and f). Water bodies and urban areas were excluded from the comparison. Model outputs were rescaled by bilinear interpolation to the resolution of the LSASAF product for comparison.

significantly between the moderate 2012 drought (2017 event excluded due to missing TWS data) and the severe 2022 drought (r = 0.77, Figure S7). Across the study sub-catchments, the observed annual imbalance was 69±234 mm in 2012, 51±202 mm in 2022, and 108±244 mm on average over the whole study period.

3.4 Impact of calibration period on model performances during the severe drought

Including a moderate drought (the 2017 event) in the calibration period did not improve model skills during the severe drought (2022). Model performance during calibration was similar during both calibration experiments (Section 2.4.1), with a mean KGE across the calibrated sub-catchments = 0.58 for calibration 1 and 0.44 for calibration 2 (Table S4). Also for the model calibrated during a drought, Q simulation performances across the study sub-catchments deteriorated significantly during the severe 2022 drought compared to model skills during moderate droughts (KGE = 0.5±0.27 during moderate droughts vs 0.18±0.63 during the severe drought, Figure 7c). Furthermore, the model calibrated during a moderate drought showed issues in simulating monthly ET standardized anomalies in the croplands during the severe drought, with mean r = -0.11 and mean nRMSE = 1.78 across the cropland model cells (Figure 7f and i), similarly to the model calibrated during average climatic conditions.

4 Discussion

4.1 Main findings in context

We investigated the skills of the distributed and process-based hydrological model Continuum in simulating streamflow (Q) under droughts of varying severity over the Po river basin in Italy, we explored possible causes for the decrease in model performances we detected for the severe 2022 drought, and we tested the benefit of including a moderate drought in the calibration period.

Over the whole study period, we achieved a satisfactory Q simulation even in a heavily human-affected area (mean KGE = 0.7 across the 38 study sub-catchments, Table S4), consistently to [47] who applied the model over the study area previously. Focusing on specific climatic periods, we found that Continuum represented Q reasonably well during moderate droughts such as the 2012 and 2017 events (KGE = 0.55±0.25, as mean ± standard deviation across the sub-catchments, Figure 3b). During the severe 2022 drought, the model simulated Q still reliably for the basin outlet (KGE = 0.82), which had the highest weight in the calibration procedure (Section 2.4.2). However, we revealed a decrease in model performances across the other study sub-catchments during 2022 (KGE = 0.18±0.69, Figure 3c), with a general overestimation of

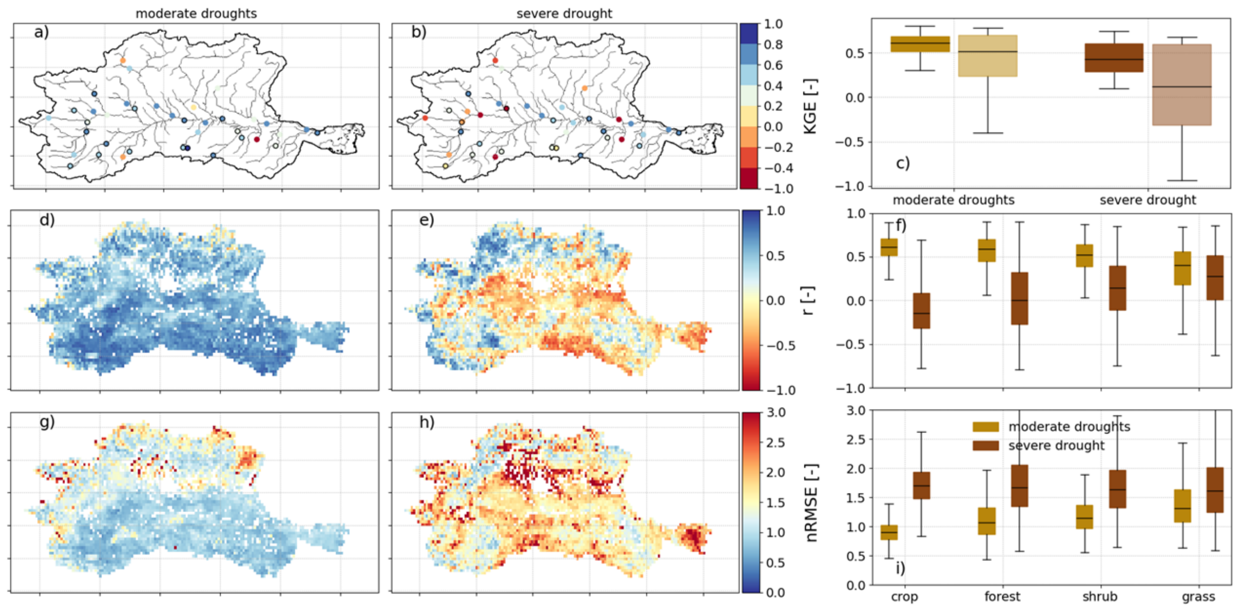

Figure 7: Summary of model performances for the model calibrated during a drought: KGE values on monthly Q over moderate droughts (a) and the severe drought (b) for each study sub-catchment, their distributions as boxplots (c) grouped by calibration (full colours) and evaluation (light colours) sub-catchments, maps of r and nRMSE on monthly ET standardized anomalies over moderate droughts (d and g) and the severe drought (e and h), and errors distributions as boxplots per each land cover types (f and i). Water bodies and urban areas were excluded from the comparison. Model outputs were rescaled by bilinear interpolation to the resolution of the LSASAF product for comparison.

Q (Figure S4). On the one hand, our results showed the ability of Continuum in simulating Q during moderate droughts, even for a model variant calibrated during average climatic conditions (Section 2.4.1). [27] found indeed that a distributed hydrological model outperformed lumped and semi-distributed models in their transferability outside the climatic conditions of the calibration period. On the other hand, we found an overestimation of Q across the study sub-catchments during the 2022 event that points to room for possible model improvement during severe droughts, as reported also by studies for conceptual models during prolonged and particularly severe droughts, such as the Millennium Drought in Australia [26] and the Californian multi-year drought between 2012 and 2016 [28].

Focusing on the overestimation of Q during the severe drought, potential causes for this could be (i) an underestimation of simulated ET, (ii) an overestimation of simulated TWS contribution to Q, and (iii) inconsistencies in the data used to force/evaluate the model. We indeed found that model capability in simulating spatial and temporal variability of ET decreased significantly during the severe drought compared to moderate droughts, especially in the human-affected areas with mean r = -0.03 and mean nRMSE = 1.74 across the croplands in 2022 (Figure 6). An overestimation of simulated TWS contribution to Q could arise from an (under-) overestimation of the (final) initial storage conditions. We showed that the model overestimated slightly TWS over the basin both at the beginning and the end of 2022 (Figure 4g), and thus it underestimated slightly its contribution to Q, rather than overestimating it. Finally, inconsistencies in observed data could stem either from an overestimation of P or an underestimation of Q, due to increased uncertainty in the measurements under extremely low flow conditions [69] for instance. A slightly positive observed imbalance could contribute to an overestimation in Q for some sub-catchments, but we did not detect any systematic increase across the study sub-catchments during 2022 compared to the moderate 2012 drought (observed imbalance between ingoing and outgoing water fluxes = 69±234 mm in 2012 and 51±202 mm in 2022, Figure S7). Therefore, we identified the misrepresentation of ET - and its underestimation in particular (Figure 4) - as the main cause for Q overestimation during the severe drought. Previous studies showed indeed that a poor ET simulation can hamper Q simulation during severe droughts [28], and ET has a prominent role particularly during severe and prolonged events [70, 71]. Specifically for the 2022 drought over the Po river basin, [68] found that the summer Q deficit was the most severe over the past two centuries and part of a declining trend in low flows (see also Figure 4a) which they related to changes in P seasonality, and increases in ET and irrigated areas. Thus, they argued ET and human activities as potential drivers of the 2022 drought and land use changes as a driver of changes in ET. [72] further showed increases in ET in the region over the last two decades from an ensemble of remote sensing-based products and they mainly attributed them to climatic changes, in particular to increases in the atmospheric evaporative demand. While proper attributions of the Q deficit in summer 2022 and the increases in ET over recent years to their multiple potential drivers, including human activities, would require high-resolution data on water withdrawals for irrigation which are currently not available [68], model difficulties in representing ET during 2022 may further point to positive ET anomalies as one of the factors contributing to the severe 2022 drought over the Po river basin. Specifically, the model misrepresentation of ET during this event could derive from (i) the model neglection of irrigation, which could have strongly increased water availability for ET during the exceptionally dry and warm summer 2022 [38], and (ii) uncertainties in model structure and parameterization for water-limited ET conditions. This latter cause would be also in line with the earlier ET suppression we detected in the simulated ET annual cycle compared to the one from the remote sensing-based ET product (Figure 4e).

Including a moderate drought (the 2017 event) in the calibration did not lead to an improvement in Q nor in ET during a severe drought (the 2022 event), with KGE = 0.18±0.63 for Q across the study sub-catchments, and mean r = -0.11 and nRMSE = 1.78 for ET across the croplands in 2022 (Figure 7). This points to the uniqueness of hydroclimatological conditions and human-water interactions over the study area for the 2022 [68]. It further suggests that enhancements in the representation of these processes in the model, rather than in model parameterization, could be beneficial to improve the simulation during severe droughts. [16] tested different calibration strategies for an ecohydrological model for the modelling of the 2018–2019 German drought in an experimental catchment and they reported an improvement in model performances by including the drought in the calibration period, compared to those from an alternative calibration period. While acknowledging that different experimental designs, study areas, models, and calibration procedures could lead to partly contrasting results, our findings complement those from [16], by demonstrating that calibrating during a drought may not be sufficient to ensure model transferability to a different and more severe drought.

4.2 Implications for hydrological modelling in a changing climate and the Anthropogenic era

The outcomes of this study have relevant implications for operational applications and scientific developments. A satisfactory representation of Q timing, even during a severe drought (Figure S5), is encouraging for drought monitoring tools for instance, whereas the overestimation of Q during the severe 2022 drought could stand for a potential underestimation of the severity of predicted extreme droughts in climate impact assessments. By identifying most plausible causes for this Q overestimation during the severe drought, our results set directions for future research to increase model robustness also during severe events (Section 4.3). Recent literature revealed that a changing climate may exacerbate the occurrence of severe and prolonged droughts [17]. Thus, our results are highly relevant in a changing climate.

Furthermore, many regions experience heavy human interference on the hydrological cycle today, via flow regulation and water withdrawals for instance [20], similarly to the Po river basin. However, these activities are generally neglected or highly simplified in hydrological models [22], mostly due to the difficulty to obtain data on them at large scales. Global-scale products on major reservoirs, such as those provided by [49], allow to represent flow regulation in hydrological models, even though in a simplified way. Yet, water withdrawals, including those for irrigation, are generally neglected, especially in catchment hydrological models. By identifying the neglection of irrigation in the model as a possible cause for ET underestimation and the consequent Q overestimation during the severe 2022 drought over the Po river basin, our study highlights the need for improvements in the representation of human activities in hydrological models to move towards more robust simulations during severe droughts in the Anthropogenic era (Section 4.3).

4.3 Future directions

Our study area encompassed a variety of climates and land cover types (Figure 1), and our study period included droughts of various severity (Figure 2). Nevertheless, our results referred to a particular model over a specific region and specific drought events. Intercomparison studies over different areas and events would help to generalize our conclusions.

In this work, we showed the usefulness of remote sensing-based products as benchmarks for distributed models to unravel their potential pitfalls. However, ET and TWS retrieval through remote sensing still presents challenges, as we cannot measure ET directly and we can derive TWS anomalies only at large scales. Therefore, part of the model errors we identified may be attributable to the benchmark datasets used for model evaluation. For TWS, we applied the mean of three latest GRACE products (Section 2.3.2) to take into account uncertainties [59]. As ET dataset, we exploited the LSASAF product, which showed skilful performances over the study area, even during droughts [50]. Benchmarking the model against alternative additional datasets for ET or other variables, such as soil moisture and snow, would be beneficial to further assess model internal consistency during droughts.

Multivariable calibration can be helpful to improve model internal consistency [73, 74], also during low-flow periods [75] and droughts [16]. [16] for example showed that including tracer data in the calibration of an ecohydrological model increased process consistency during the 2018–2019 drought in Central Europe. Here we calibrated the model against Q data only (Section 2.4.2). Given the satisfactory performances we achieved for ET during moderate droughts, we argue that a multi-variable calibration approach will probably not enhance significantly model performances outside the calibration conditions. [76] showed that a multi-objective calibration with Q data aggregated at different time scales improved Q transferability outside the calibration conditions for a distributed model in a German medium-sized basin. Future work could test similar multi-objective or multi-variable approaches, in the latter case by possibly exploiting spatial metrics (see e.g., [73]) to consider also spatial information on additional hydrological fluxes or states.

Human interference affects heavily the hydrological cycle in the study area, both in terms of water regulation and withdrawals (Section 2.1). Here, Continuum included flow regulation through reservoirs, although we did not know their operating rules. Yet, the model did not include water withdrawals and irrigation, which can be more relevant during droughts than during wet periods [39] and are often neglected in hydrological models [22]. By calibrating the model against observed Q data, model parameterization partly accounts for the effects of human interference. However, an enhanced representation of human interference could improve hydrological modelling during severe droughts. For instance, [77] achieved a median 10.6% improvement in low-flows simulation by including data on monthly withdrawals and releases in a distributed hydrological model for 605 catchments in England. [78] proposed effective techniques to derive remote sensing-based irrigation estimates that can be incorporated into distributed hydrological modelling. Further research should investigate the benefits of assimilating these kind of new data in the representation of the human-affected hydrological cycle during severe droughts.

5 Conclusions

We evaluated model performances during droughts of different severity for the distributed hydrological model Continuum over the heavily human-affected Po river basin in northern Italy. By using ground- and remote sensing-based independent benchmarks of Q, ET, and TWS anomalies, we investigated potential causes of model deterioration during the severe 2022 drought. Furthermore, we tested if calibrating during a moderate drought could be an effective strategy to improve model performances during a severe drought. We revealed that even a model that does not show decreased performances for moderate droughts may do so during a severe drought (Figure 3). We linked Q overestimation during the severe drought to an underestimation of ET, mainly in the irrigated croplands (Figure 6). Moreover, we demonstrated that including a moderate drought in the calibration was not sufficient to improve Q and ET simulation during a severe drought (Figure 7). Based on our findings, we highlight the need for holistic model evaluations, as well as model developments to enhance the representation of human activities (e.g., by including irrigation fluxes) in distributed hydrological models, with the ultimate goal of increasing model robustness during severe droughts. Considering the expected exacerbation of droughts in a changing climate, the heavy human interference on many hydrological systems today, and the generally oversimplification of human activities in hydrological models, these results are highly relevant to properly inform water management and climate adaptation strategies.

CRediT authorship contribution statement

Giulia Bruno: Conceptualization, Methodology, Software, Formal Analysis, Investigation, Writing- Original draft preparation, Visualization. Francesco Avanzi: Conceptualization, Writing- Reviewing and Editing. Lorenzo Alfieri: Software, Writing- Reviewing and Editing. Andrea Libertino: Software, Writing- Reviewing and Editing. Simone Gabellani: Supervision, Conceptualization, Writing- Reviewing and Editing. Doris Duethmann: Supervision, Conceptualization, Writing- Reviewing and Editing.

Acknowledgments

This study was carried out within the RETURN Extended Partnership and received funding from the European Union Next-GenerationEU (National Recovery and Resilience Plan – NRRP, Mission 4, Component 2, Investment 1.3 – D.D. 1243 2/8/2022, PE0000005). This paper has been supported by the Italian Department of Civil Protection, Presidency of the Council of Ministers, through the convention between Department of Civil Protection and CIMA Research Foundation, for the development of knowledge, methodologies, technologies and training useful for the implementation of national systems of monitoring, prevention and surveillance.

A Supplementary material

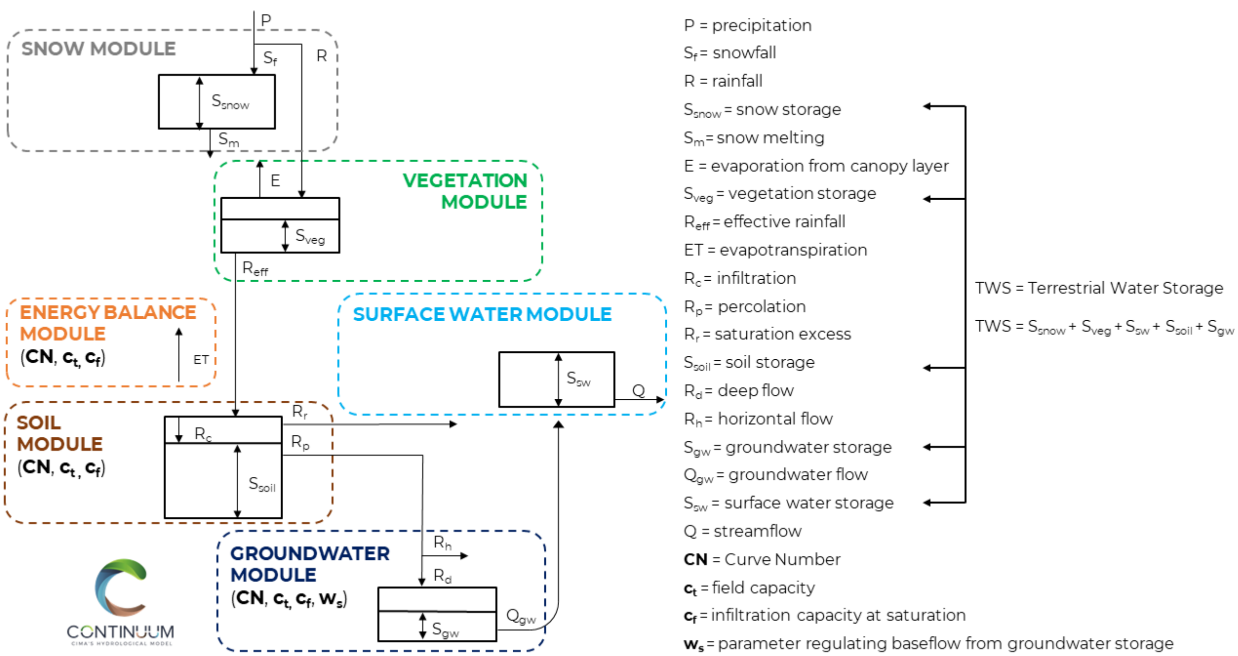

Figure S.1: Diagram of the hydrological model Continuum [34] setup in this study (Section 2.2), with considered hydrological fluxes and states, model modules, and calibration parameters (in bold, Section 2.4.2).

[1] https://landsaf.ipma.pt/en/products/evapotranspiration-energy-flxs/met/ (last access on 06 October 2022)
[2] https://podaac-tools.jpl.nasa.gov/drive/files/GeodeticsGravity/tellus/L3/mascon/RL06/JPL/v02/CRI/netcdf (last access on 06 October 2022)
[3] http://www2.csr.utexas.edu/grace/RL06_mascons.html (last access on 06 October 2022)
[4] https://earth.gsfc.nasa.gov/geo/data/grace-mascons (last access on 06 October 2022)

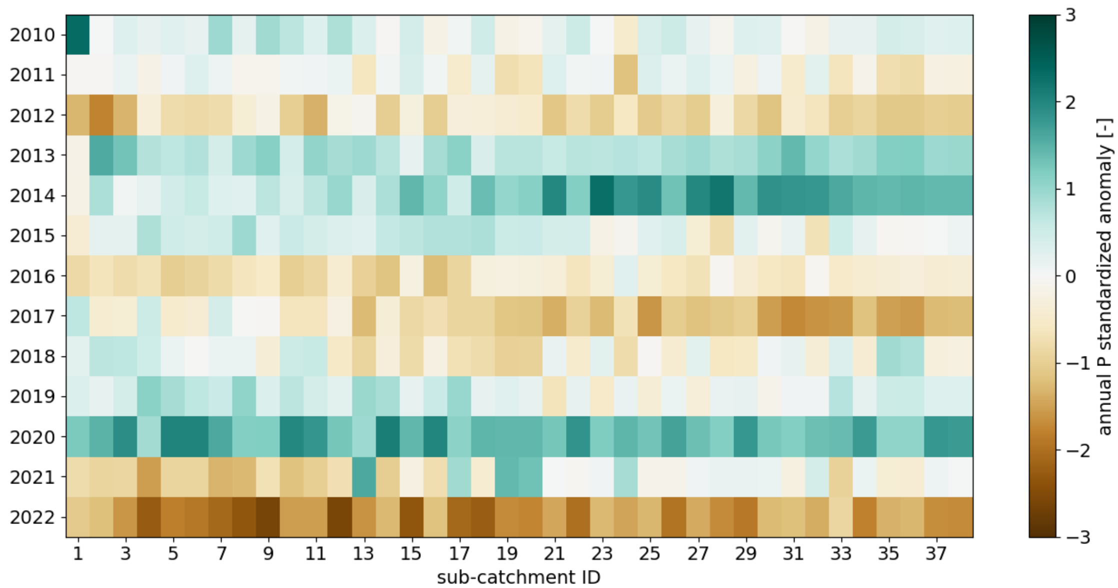

Figure S.2: Climatic conditions over the study area and period: annual precipitation (P) standardized anomalies (Equation 1) for each study sub-catchment (ordered west-to-east, from the left to the right end side) over the study period.

Table S.1: Overview of datasets used in the study.

Variable	Dataset	Reference	Purpose
Digital Elevation Model	HDMA	[40]	Model setup
Hydrological Soil Group	HYSOGs250m	[79]	Model setup
Soil texture	ISRIC SoilGrids	[80]	Model setup
Soil porosity	ESACCI Soil Moisture	[81]	Model setup
Land Cover	ESACCI 2018 Land Cover	[44]	Model setup
Dams	DPC and GranD database	[49] for GranD database	Model setup
Lakes	DPC	[47]	Model setup
Glaciers	RGIv6	[82]	Model setup
Meteo data	DPC	[48, 47]	Model simulation
Streamflow	DPC and regional hydrometeorological offices	[47, 50]	Model calibration and evaluation
Evapotranspiration	LSASAF	[51, 52][1]	Model evaluation
Terrestrial Water Storage	GRACE JPL mascon RL06	[56, 57][2]	Model evaluation
Terrestrial Water Storage	GRACE CSR mascon RL06	[54, 55][3]	Model evaluation
Terrestrial Water Storage	GRACE GSFC mascon RL06	[58][4]	Model evaluation

Table S.2: Properties of study sub-catchments: ID, name, location, drainage area [km^2], mean elevation [m a.s.l.], dominant climate and land cover type. Dominant climate was determined from [41] and other data sources are listed in Table S.1. Sub-catchments are ordered west-to-east.

ID	Section	Basin	Lat	Lon	Area [km^2]	Elev [m a.s.l.]	Climate	Land cover
1	Susa Via Mazzini	Dora Riparia	45.14	7.05	832	2120	Cold	Forest
2	Gaiola	Stura di Demonte	44.33	7.42	562	1744	Cold	Grass
3	Lanzo	Stura di Lanzo	45.27	7.48	580	1767	Cold	Grass
4	Busca	Maira	44.52	7.48	613	1514	Cold	Forest
5	Carignano	Po	44.91	7.69	3957	1021	Temperate no dry	Forest
6	Torino Murazzi	Po	45.07	7.71	5152	971	Temperate no dry	Crop
7	Torino	Dora Riparia	45.08	7.72	1475	1373	Cold	Grass
8	S.Benigno	Orco	45.25	7.81	852	1645	Cold	Grass
9	Tavagnasco	Dora Baltea	45.55	7.82	3297	2124	Alpine	Grass
10	Farigliano	Tanaro	44.52	7.9	1505	916	Temperate dry	Forest
11	Alba Q.A.	Tanaro	44.71	8.03	3468	1313	Temperate dry	Forest
12	Verolengo	Dora Baltea	45.19	8.04	3962	1802	Alpine	Grass
13	Domodossola	Toce	46.11	8.31	954	1928	Alpine	Grass
14	Piana Crixia	Bormida	44.48	8.31	249	610	Temperate dry	Forest
15	Quinto Vercellese Cervo	Sesia	45.38	8.37	840	578	Temperate no dry	Forest
16	Candoglia	Toce	45.97	8.42	1564	1896	Alpine	Grass
17	Cartosio	Erro	44.57	8.42	196	544	Temperate dry	Forest
18	Palestro	Sesia	45.30	8.51	2709	826	Temperate no dry	Forest
19	Vigevano	Ticino	45.34	8.88	7467	1453	Cold	Forest
20	Ponte della Libertà	Ticino	45.18	9.15	8378	1383	Cold	Forest
21	Valsigiara	Trebbia	44.64	9.33	209	959	Cold	Forest
22	Spessa	Po	45.10	9.35	38626	1094	Temperate no dry	Forest
23	Salsominore	Aveto	44.63	9.41	186	1060	Cold	Forest
24	Lodi	Adda	45.32	9.51	6127	1515	Cold	Forest
25	Rivergaro	Trebbia	44.9	9.58	886	820	Cold	Forest
26	Ostia Parmense	Taro	44.51	9.84	422	859	Temperate no dry	Forest
27	Piacenza	Po	45.06	9.71	42090	992	Temperate no dry	Forest
28	Capriolo	Oglio	45.64	9.92	1921	1347	Cold	Forest
29	Cremona	Po	45.13	10.00	51163	1214	Temperate no dry	Forest
30	S.Secondo	Taro	44.92	10.25	1545	645	Temperate no dry	Forest
31	Ponte Verdi	Parma	44.81	10.25	527	649	Temperate no dry	Forest
32	Marcaria	Oglio	45.11	10.53	6085	723	Temperate no dry	Crop
33	Cadelbosco	Crostolo	44.78	10.58	258	247	Temperate no dry	Crop
34	Borgoforte	Po	45.04	10.75	63575	954	Temperate no dry	Forest
35	Ponte Alto	Secchia	44.67	10.9	1174	743	Temperate no dry	Forest
36	Pioppa	Secchia	44.86	10.97	1330	661	Temperate no dry	Forest
37	Ficarolo	Po	44.95	11.43	69315	867	Temperate no dry	Forest
38	Pontelagoscuro	Po	44.89	11.61	72545	832	Temperate no dry	Forest

Table S.3: Overview of the model parameters calibrated in this study (Curve Number, CN, field capacity c_t, infiltration velocity at saturation c_f, and a parameter regulating the baseflow from the groundwater storage w_s), with indication of their type (distributed or lumped for the model domain), ranges used in the calibration, first guess and calibrated values for the two experiments, where applicable. Please refer to Figure S3 for first guess and calibrated values for distributed parameters.

Parameter	Type	Range	First guess	Calibration 1	Calibration 2
CN	distributed	[30, 99]	-	-	-
c_t	distributed	[0.1, 0.7]	-	-	-
c_f	distributed	[0.01, 0.1]	-	-	-
w_s	lumped	[10e-12, 10e-07]	3.68e-09	1.61e-08	6.04e-08

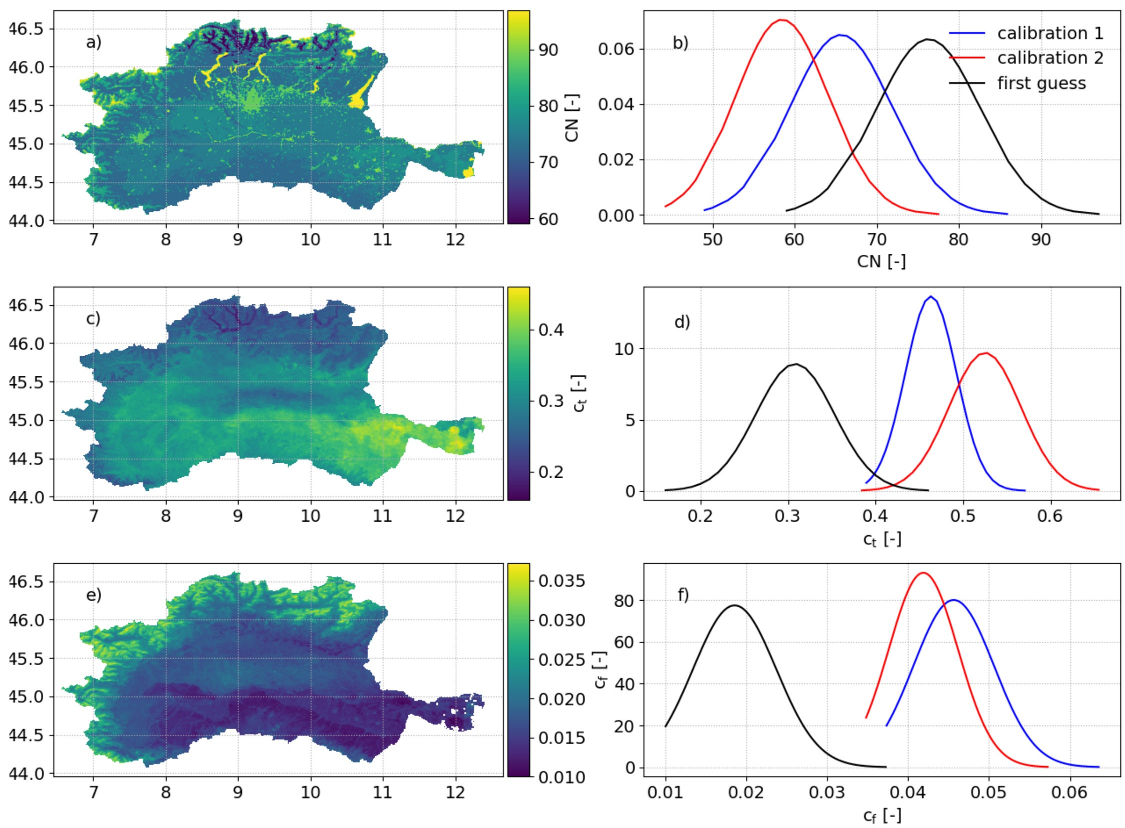

Figure S.3: Overview of the distributed model parameters we calibrated in this study (Curve Number, CN, field capacity ct, and infiltration velocity at saturation cf). (a, c, e) Maps of the first guess parameters and (b, d, f) distributions of the first guess values (black), and calibrated values (for calibration 1, blue, and 2, red). For differences between the two calibration experiments, see Section 2.4.1.

Table S.4: Streamflow (Q) model performances: Kling Gupta Efficiency (KGE [63]) for calibration and evaluation periods for each study sub-catchment (Table S.2). KGE_1 refers to calibration experiment 1 and KGE_2 refers to calibration experiment 2 (Section 2.4.1).

ID	KGE_1	$\text{KGE}_{1,\text{whole}}$	$\text{KGE}_{1,\text{wet}}$	$\text{KGE}_{1,\text{moderate}}$	$\text{KGE}_{1,\text{severe}}$	KGE_2	$\text{KGE}_{2,\text{whole}}$	$\text{KGE}_{2,\text{wet}}$	$\text{KGE}_{2,\text{moderate}}$	$\text{KGE}_{2,\text{severe}}$
1	-	0.58	0.48	0.43	0.01	-	0.53	0.46	0.49	<0
2	0.52	0.58	0.52	0.31	0.31	0.47	0.55	0.51	0.41	0.17
3	0.47	0.67	0.71	0.47	0.34	<0	0.67	0.76	0.51	0.32
4	-	0.49	0.32	0.69	0.1	-	0.63	0.49	0.59	<0
5	0.85	0.85	0.74	0.48	<0	0.74	0.82	0.88	0.67	0.63
6	0.81	0.86	0.7	0.59	0.11	0.62	0.79	0.85	0.62	0.4
7	-	0.47	0.33	0.08	<0	-	0.58	0.46	0.37	<0
8	-	0.79	0.86	0.84	<0	-	0.76	0.81	0.76	<0
9	0.71	0.74	0.67	0.72	0.65	0.7	0.69	0.63	0.68	0.6
10	0.84	0.81	0.85	0.64	0.43	0.58	0.76	0.84	0.56	0.28
11	0.79	0.89	0.79	0.71	0.07	0.59	0.85	0.81	0.62	0.57
12	-	0.39	0.34	0.29	<0	-	0.45	0.36	0.28	<0
13	-	0.38	0.37	<0	<0	-	0.39	0.38	<0	<0
14	-	0.28	0.29	0.28	<0	-	0.02	0.01	<0	<0
15	-	0.54	0.43	0.2	0.51	-	0.63	0.61	0.71	0.68
16	-	0.55	0.45	0.5	0.19	-	0.57	0.51	0.55	0.26
17	0.55	0.83	0.96	0.9	0.46	0.25	0.7	0.87	0.52	0.39
18	0.74	0.7	0.52	0.84	<0	0.08	0.6	0.44	0.6	¡0
19	-	0.85	0.79	0.71	0.77	-	0.79	0.73	0.78	0.62
20	-	0.89	0.74	0.75	0.77	-	0.84	0.64	0.76	0.64
21	0.46	0.89	0.91	0.69	0.47	<0	0.82	0.92	0.6	0.27
22	0.87	0.85	0.71	0.76	0.7	0.84	0.89	0.91	0.76	0.64
23	<0	0.4	<0	0.59	<0	0.67	0.35	<0	0.8	0.1
24	-	0.77	0.76	0.32	0.66	-	0.74	0.82	0.06	0.59
25	-	0.78	0.73	0.64	<0	-	0.84	0.77	0.58	0.37
26	0.54	0.94	0.89	0.83	0.82	0.2	0.89	0.88	0.77	0.74
27	-	0.88	0.76	0.72	0.68	-	0.87	0.89	0.76	0.61
28	-	0.44	0.39	0.16	<0	-	0.51	0.49	0.21	<0
29	0.81	0.78	0.68	0.71	0.83	0.78	0.91	0.95	0.76	0.61
30	0.46	0.81	0.86	0.71	0.51	0.25	0.69	0.76	0.36	0.61
31	0.23	0.67	0.76	0.69	0.42	0.44	0.57	0.72	0.46	0.38
32	-	0.67	0.56	0.46	<0	-	0.63	0.53	0.24	<0
33	-	0.34	<0	<0	<0	-	0.14	<0	<0	<0
34	-	0.81	0.66	0.72	0.85	-	0.88	0.96	0.69	0.67
35	0.67	0.81	0.83	0.43	0.65	0.12	0.67	0.81	0.3	0.46
36	-	0.78	0.87	0.52	0.76	-	0.62	0.74	0.38	0.49
37	-	0.83	0.63	0.74	0.81	-	0.86	0.95	0.65	0.61
38	0.79	0.81	0.58	0.77	0.82	0.71	0.88	0.94	0.64	0.64

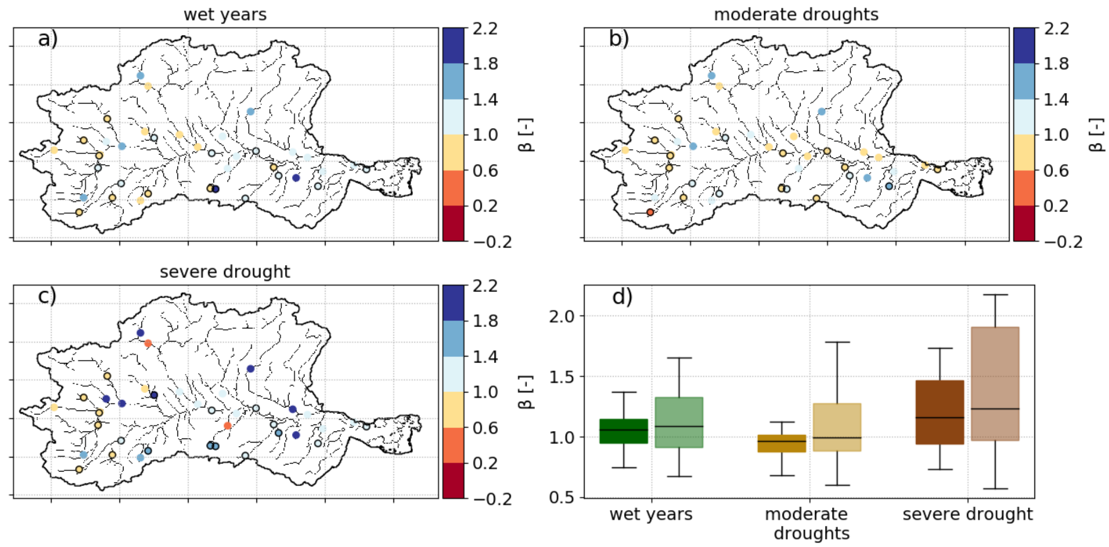

Figure S.4: Streamflow (Q) model performances from the model calibrated during average climatic conditions (2.4.1): values of the bias component (β) of the Kling Gupta Efficiency (KGE [63], Equation 2) on monthly Q during (a) wet years, (b) moderate droughts, and (c) the severe drought for each study sub-catchment, and (d) their distributions as boxplots, grouped by calibration (full colours) and evaluation (light colours) sub-catchments.

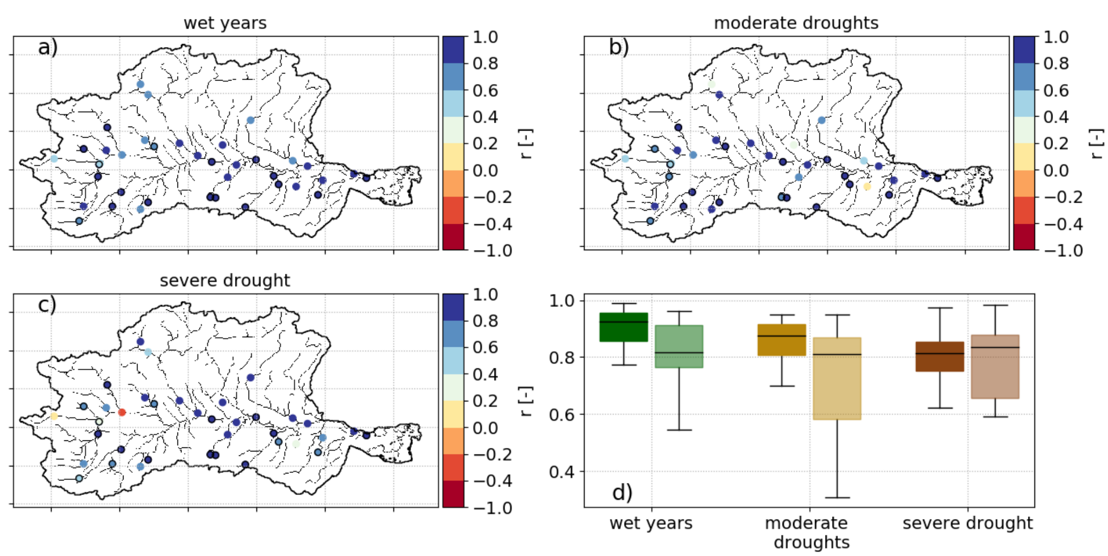

Figure S.5: Same as S.4, but for the timing component (r) of KGE (Equation 2).

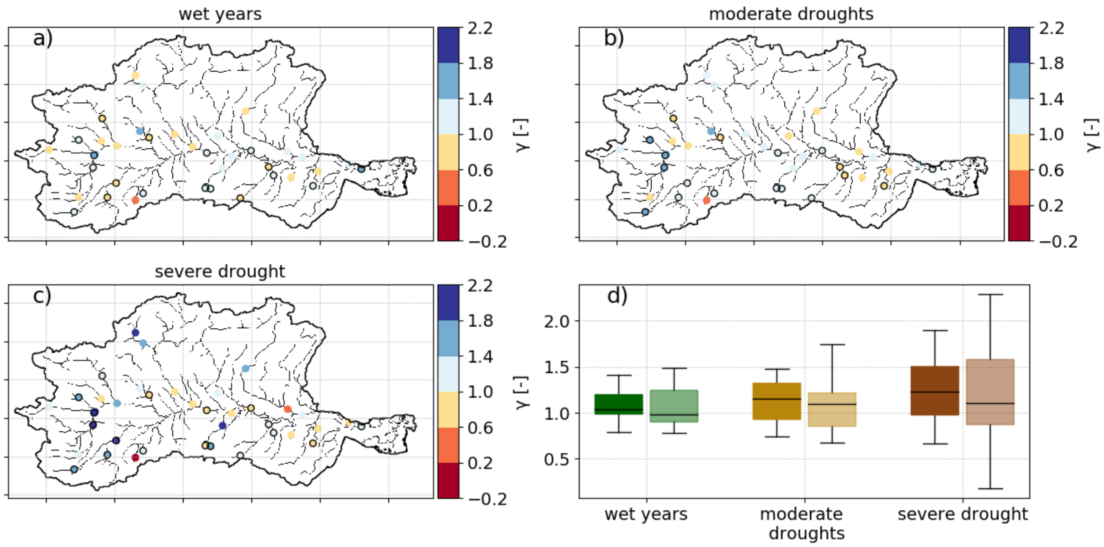

Figure S.6: Same as S.4, but for the variability component (γ) of KGE (Equation 2).

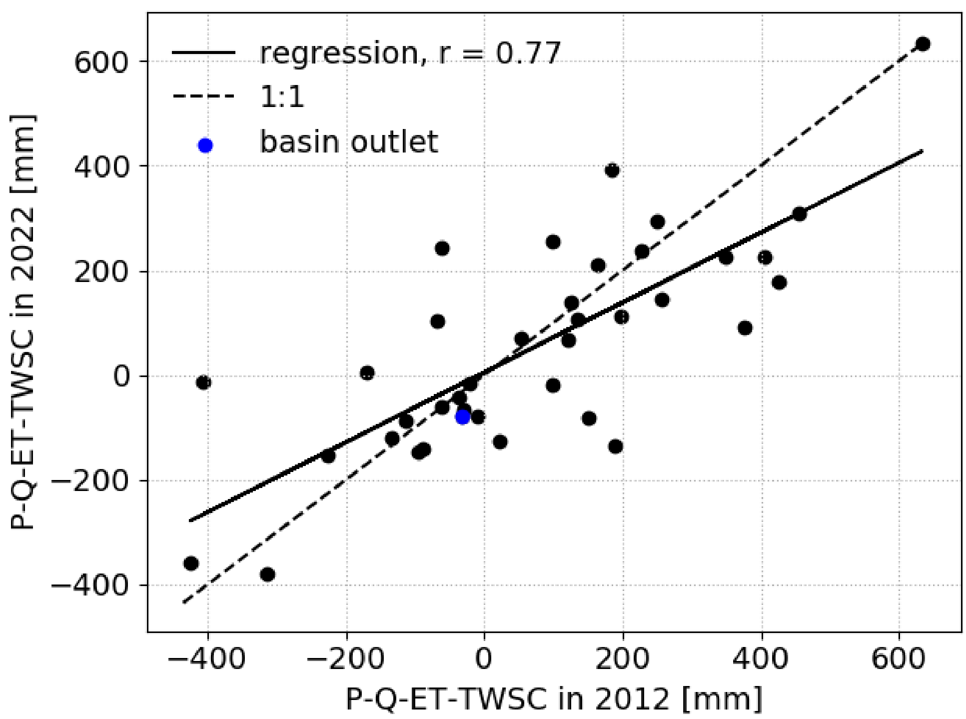

Figure S.7: Potential data inconsistencies: scatterplot between the observed water imbalance (Section 2.3.3) for each study sub-catchment (black dots) and the basin outlet (blue dot) in 2012 and 2022. P, Q, ET, and TWSC are the annual precipitation, streamflow, evapotranspiration, and changes in Terrestrial Water Storage.

References

[1] Anne F Van Loon. Hydrological drought explained. *Wiley Interdisciplinary Reviews: Water*, 2(4):359–392, 2015.

[2] UNDRR. Gar special report on drought 2021. 2021.

[3] Gustavo Naumann, Carmelo Cammalleri, Lorenzo Mentaschi, and Luc Feyen. Increased economic drought impacts in europe with anthropogenic warming. *Nature Climate Change*, 11(6):485–491, 2021.

[4] Simone Fatichi, Enrique R Vivoni, Fred L Ogden, Valeriy Y Ivanov, Benjamin Mirus, David Gochis, Charles W Downer, Matteo Camporese, Jason H Davison, Brian Ebel, et al. An overview of current applications, challenges, and future trends in distributed process-based models in hydrology. *Journal of Hydrology*, 537:45–60, 2016.

[5] Marc FP Bierkens, Victoria A Bell, Peter Burek, Nathaniel Chaney, Laura E Condon, Cédric H David, Ad de Roo, Petra Döll, Niels Drost, James S Famiglietti, et al. Hyper-resolution global hydrological modelling: what is next? "everywhere and locally relevant". *Hydrological processes*, 29(2):310–320, 2015.

[6] MHJ Van Huijgevoort, HAJ Van Lanen, AJ Teuling, and R Uijlenhoet. Identification of changes in hydrological drought characteristics from a multi-gcm driven ensemble constrained by observed discharge. *Journal of Hydrology*, 512:421–434, 2014.

[7] Carmelo Cammalleri, Gustavo Naumann, Lorenzo Mentaschi, Bernard Bisselink, Emiliano Gelati, Ad De Roo, and Luc Feyen. Diverging hydrological drought traits over europe with global warming. *Hydrology and Earth System Sciences*, 24(12):5919–5935, 2020.

[8] Moctar Dembélé, Mathieu Vrac, Natalie Ceperley, Sander J Zwart, Josh Larsen, Simon J Dadson, Grégoire Mariéthoz, and Bettina Schaefli. Contrasting changes in hydrological processes of the volta river basin under global warming. *Hydrology and earth system sciences*, 26(5):1481–1506, 2022.

[9] Carmelo Cammalleri, Jürgen Vogt, and Peter Salamon. Development of an operational low-flow index for hydrological drought monitoring over europe. *Hydrological Sciences Journal*, 62(3):346–358, 2017.

[10] C Cammalleri, P Barbosa, and JV Vogt. Evaluating simulated daily discharge for operational hydrological drought monitoring in the global drought observatory (gdo). *Hydrological Sciences Journal*, 65(8):1316–1325, 2020.

[11] Toma Rani Saha, Pallav K Shrestha, Oldrich Rakovec, Stephan Thober, and Luis Samaniego. A drought monitoring tool for south asia. *Environmental Research Letters*, 16(5):054014, 2021.

[12] P Trambauer, M Werner, HC Winsemius, S Maskey, E Dutra, and S Uhlenbrook. Hydrological drought forecasting and skill assessment for the limpopo river basin, southern africa. *Hydrology and Earth System Sciences*, 19(4):1695–1711, 2015.

[13] Theresa C Van Hateren, Samuel J Sutanto, and Henny AJ Van Lanen. Evaluating skill and robustness of seasonal meteorological and hydrological drought forecasts at the catchment scale–case catalonia (spain). *Environment international*, 133:105206, 2019.

[14] Samuel J Sutanto, Fredrik Wetterhall, and Henny AJ Van Lanen. Hydrological drought forecasts outperform meteorological drought forecasts. *Environmental Research Letters*, 15(8):084010, 2020.

[15] Theodoros Mastrotheodoros, Christoforos Pappas, Peter Molnar, Paolo Burlando, Gabriele Manoli, Juraj Parajka, Riccardo Rigon, Borbala Szeles, Michele Bottazzi, Panagiotis Hadjidoukas, et al. More green and less blue water in the alps during warmer summers. *Nature Climate Change*, 10(2):155–161, 2020.

[16] Xiaoqiang Yang, Doerthe Tetzlaff, Chris Soulsby, Aaron Smith, and Dietrich Borchardt. Catchment functioning under prolonged drought stress: Tracer-aided ecohydrological modeling in an intensively managed agricultural catchment. *Water Resources Research*, 57(3):e2020WR029094, 2021.

[17] Oldrich Rakovec, Luis Samaniego, Vittal Hari, Yannis Markonis, Vojtěch Moravec, Stephan Thober, Martin Hanel, and Rohini Kumar. The 2018–2020 multi-year drought sets a new benchmark in europe. *Earth's Future*, 10(3):e2021EF002394, 2022.

[18] Amit Kumar, Simon N Gosling, Matthew F Johnson, Matthew D Jones, Jamal Zaherpour, Rohini Kumar, Guoyong Leng, Hannes Müller Schmied, Jenny Kupzig, Lutz Breuer, et al. Multi-model evaluation of catchment-and global-scale hydrological model simulations of drought characteristics across eight large river catchments. *Advances in Water Resources*, page 104212, 2022.

[19] AF Van Loon, MHJ Van Huijgevoort, and HAJ Van Lanen. Evaluation of drought propagation in an ensemble mean of large-scale hydrological models. *Hydrology and Earth System Sciences*, 16(11):4057–4078, 2012.

[20] Benjamin W Abbott, Kevin Bishop, Jay P Zarnetske, David M Hannah, Rebecca J Frei, Camille Minaudo, F Stuart Chapin, Stefan Krause, Lafe Conner, David Ellison, et al. A water cycle for the anthropocene. *Hydrological Processes*, 33(23), 2019.

[21] Anne F Van Loon, Sally Rangecroft, Gemma Coxon, Micha Werner, Niko Wanders, Giuliano Di Baldassarre, Erik Tijdeman, Marianne Bosman, Tom Gleeson, Alexandra Nauditt, et al. Streamflow droughts

aggravated by human activities despite management. *Environmental Research Letters*, 17(4):044059, 2022.

[22] Yoshihide Wada, Marc FP Bierkens, Ad De Roo, Paul A Dirmeyer, James S Famiglietti, Naota Hanasaki, Megan Konar, Junguo Liu, Hannes Müller Schmied, Taikan Oki, et al. Human–water interface in hydrological modelling: current status and future directions. *Hydrology and Earth System Sciences*, 21(8):4169–4193, 2017.

[23] Vit Klemeš. Operational testing of hydrological simulation models. *Hydrological sciences journal*, 31(1):13–24, 1986.

[24] CZ Li, L Zhang, H Wang, YQ Zhang, FL Yu, and DH Yan. The transferability of hydrological models under nonstationary climatic conditions. *Hydrology and Earth System Sciences*, 16(4):1239–1254, 2012.

[25] Doris Duethmann, Günter Blöschl, and Juraj Parajka. Why does a conceptual hydrological model fail to correctly predict discharge changes in response to climate change? *Hydrology and Earth System Sciences*, 24(7):3493–3511, 2020.

[26] Margarita Saft, Murray C Peel, Andrew W Western, Jean-Michel Perraud, and Lu Zhang. Bias in streamflow projections due to climate-induced shifts in catchment response. *Geophysical Research Letters*, 43(4):1574–1581, 2016.

[27] Proloy Deb and Anthony S Kiem. Evaluation of rainfall–runoff model performance under non-stationary hydroclimatic conditions. *Hydrological Sciences Journal*, 65(10):1667–1684, 2020.

[28] Francesco Avanzi, Joseph Rungee, Tessa Maurer, Roger Bales, Qin Ma, Steven Glaser, and Martha Conklin. Climate elasticity of evapotranspiration shifts the water balance of mediterranean climates during multi-year droughts. *Hydrology and Earth System Sciences*, 24(9):4317–4337, 2020.

[29] Seth Westra, Mark Thyer, Michael Leonard, Dmitri Kavetski, and Martin Lambert. A strategy for diagnosing and interpreting hydrological model nonstationarity. *Water Resources Research*, 50(6):5090–5113, 2014.

[30] Keirnan Fowler, Wouter Knoben, Murray Peel, Tim Peterson, Dongryeol Ryu, Margarita Saft, Ki-Weon Seo, and Andrew Western. Many commonly used rainfall-runoff models lack long, slow dynamics: Implications for runoff projections. *Water Resources Research*, 56(5):e2019WR025286, 2020.

[31] Danlu Guo, Seth Westra, and Holger R Maier. Impact of evapotranspiration process representation on runoff projections from conceptual rainfall-runoff models. *Water Resources Research*, 53(1):435–454, 2017.

[32] Oldrich Rakovec, Rohini Kumar, Juliane Mai, Matthias Cuntz, Stephan Thober, Matthias Zink, Sabine Attinger, David Schäfer, Martin Schrön, and Luis Samaniego. Multiscale and multivariate evaluation of water fluxes and states over european river basins. *Journal of Hydrometeorology*, 17(1):287–307, 2016.

[33] Silvana Bolaños Chavarría, Micha Werner, Juan Fernando Salazar, and Teresita Betancur Vargas. Benchmarking global hydrological and land surface models against grace in a medium-sized tropical basin. *Hydrology and Earth System Sciences*, 26(16):4323–4344, 2022.

[34] F Silvestro, S Gabellani, F Delogu, R Rudari, and G Boni. Exploiting remote sensing land surface temperature in distributed hydrological modelling: the example of the continuum model. *Hydrology and Earth System Sciences*, 17(1):39–62, 2013.

[35] D. Masante, J. Vogt, N. McCormick, C. Cammalleri, D. Magni, and A. de Jager. Severe drought in italy – july 2017. 2017.

[36] Chiara Marchina, Claudio Natali, and Gianluca Bianchini. The po river water isotopes during the drought condition of the year 2017. *Water*, 11(1):150, 2019.

[37] A. Toreti, D. Bavera, F. Avanzi, C. Cammalleri, M. De Felice, A. de Jager, C. Di Ciollo, M. Gardella, S. Gabellani, P. Leoni, W. Maetens, D. Magni, Manfron G., D. Masante, M. Mazzeschi, N. McCormick, G. Naumann, S. Niemeyer, L. Rossi, L. Seguini, J. Spinoni, and M. van den Berg. Drought in europe april 2022. (JRC129395), 2022.

[38] A. Toreti, D. Bavera, J. Acosta Navarro, C. Cammalleri, A. de Jager, C. Di Ciollo, A. Hrast Essenfelder, W. Maetens, D. Magni, D. Masante, M. Mazzeschi, S. Niemeyer, and J. Spinoni. Drought in europe august 2022. (JRC130493), 2022.

[39] Po River Basin Authority. Caratteristiche del bacino del fiume po e primo esame dell' impatto ambientale delle attivitá umane sulle risorse idriche (characteristics of po river basin and first analysis of the impact of human activities on water resources). 2006.

[40] Kristine L Verdin. Hydrologic derivatives for modeling and analysis—a new global high-resolution database. Technical report, US Geological Survey, 2017.

[41] Hylke E Beck, Niklaus E Zimmermann, Tim R McVicar, Noemi Vergopolan, Alexis Berg, and Eric F Wood. Present and future köppen-geiger climate classification maps at 1-km resolution. *Scientific data*, 5(1):1–12, 2018.

[42] A Crespi, M Brunetti, G Lentini, and M Maugeri. 1961–1990 high-resolution monthly precipitation climatologies for italy. *International Journal of Climatology*, 38(2):878–895, 2018.

[43] Francesco Avanzi, Simone Gabellani, Fabio Delogu, Francesco Silvestro, Flavio Pignone, Giulia Bruno, Luca Pulvirenti, Giuseppe Squicciarino, Elisabetta Fiori, Lauro Rossi, et al. It-snow: a snow reanalysis for italy blending modeling, in-situ data, and satellite observations (2010–2021). *Earth System Science Data Discussions*, pages 1–30, 2022.

[44] ESA. Land cover cci product user guide version 2. tech. rep. Technical report, 2017.

[45] F Silvestro, S Gabellani, R Rudari, F Delogu, P Laiolo, and G Boni. Uncertainty reduction and parameter estimation of a distributed hydrological model with ground and remote-sensing data. *Hydrology and Earth System Sciences*, 19(4):1727–1751, 2015.

[46] Francesco Silvestro, Giulia Ercolani, Simone Gabellani, Pietro Giordano, and Marco Falzacappa. Improving real-time operational streamflow simulations using discharge data to update state variables of a distributed hydrological model. *Hydrology Research*, 52(6):1239–1260, 2021.

[47] Lorenzo Alfieri, Francesco Avanzi, Fabio Delogu, Simone Gabellani, Giulia Bruno, Lorenzo Campo, Andrea Libertino, Christian Massari, Angelica Tarpanelli, Dominik Rains, et al. High-resolution satellite products improve hydrological modeling in northern italy. *Hydrology and Earth System Sciences*, 26(14):3921–3939, 2022.

[48] Giulia Bruno, Flavio Pignone, Francesco Silvestro, Simone Gabellani, Federico Schiavi, Nicola Rebora, Pietro Giordano, and Marco Falzacappa. Performing hydrological monitoring at a national scale by exploiting rain-gauge and radar networks: The italian case. *Atmosphere*, 12(6):771, 2021.

[49] Bernhard Lehner, Catherine Reidy Liermann, Carmen Revenga, Charles Vörösmarty, Balazs Fekete, Philippe Crouzet, Petra Döll, Marcel Endejan, Karen Frenken, Jun Magome, et al. High-resolution mapping of the world's reservoirs and dams for sustainable river-flow management. *Frontiers in Ecology and the Environment*, 9(9):494–502, 2011.

[50] Giulia Bruno, Francesco Avanzi, Simone Gabellani, Luca Ferraris, Edoardo Cremonese, Marta Galvagno, and Christian Massari. Disentangling the role of subsurface storage in the propagation of drought through the hydrological cycle. *Advances in Water Resources*, 169:104305, 2022.

[51] Nicolas Ghilain, Alirio Arboleda, and Françoise Gellens-Meulenberghs. Evapotranspiration modelling at large scale using near-real time msg seviri derived data. *Hydrology and Earth System Sciences*, 15(3):771–786, 2011.

[52] Algorithm Theoretical Basis Document, LSA-SAF ETv2 HLE, version 1.1. Technical report, EUMETSAT, 2016.

[53] Bridget R Scanlon, Zizhan Zhang, Himanshu Save, David N Wiese, Felix W Landerer, Di Long, Laurent Longuevergne, and Jianli Chen. Global evaluation of new grace mascon products for hydrologic applications. *Water Resources Research*, 52(12):9412–9429, 2016.

[54] Himanshu Save, Srinivas Bettadpur, and Byron D Tapley. High-resolution csr grace rl05 mascons. *Journal of Geophysical Research: Solid Earth*, 121(10):7547–7569, 2016.

[55] Himanshu Save. Csr grace and grace-fo rl06 mascon solutions v02. 2020.

[56] Michael M Watkins, David N Wiese, Dah-Ning Yuan, Carmen Boening, and Felix W Landerer. Improved methods for observing earth's time variable mass distribution with grace using spherical cap mascons. *Journal of Geophysical Research: Solid Earth*, 120(4):2648–2671, 2015.

[57] D. N. Wiese, D.-N. Yuan, C. Boening, F. W. Landerer, and M. M. Watkins. Jpl grace mascon ocean, ice, and hydrology equivalent water height rl06 cri filtered version 02. ver. 02. po.daac, ca, usa. dataset accessed [2022-08-03]. 2019.

[58] BD Loomis, SB Luthcke, and TJ Sabaka. Regularization and error characterization of grace mascons. *Journal of geodesy*, 93(9):1381–1398, 2019.

[59] BR Scanlon, Z Zhang, A Rateb, A Sun, D Wiese, H Save, H Beaudoing, MH Lo, H Müller-Schmied, P Döll, et al. Tracking seasonal fluctuations in land water storage using global models and grace satellites. *Geophysical Research Letters*, 46(10):5254–5264, 2019.

[60] Wenchao Sun, Yuanyuan Wang, Guoqiang Wang, Xingqi Cui, Jingshan Yu, Depeng Zuo, and Zongxue Xu. Physically based distributed hydrological model calibration based on a short period of streamflow data: case studies in four chinese basins. *Hydrology and Earth System Sciences*, 21(1):251–265, 2017.

[61] Laura Poggio, Luis M De Sousa, Niels H Batjes, Gerard Heuvelink, Bas Kempen, Eloi Ribeiro, and David Rossiter. Soilgrids 2.0: producing soil information for the globe with quantified spatial uncertainty. *Soil*, 7(1):217–240, 2021.

[62] Michael D McKay, Richard J Beckman, and William J Conover. A comparison of three methods for selecting values of input variables in the analysis of output from a computer code. *Technometrics*, 42(1):55–61, 2000.

[63] Harald Kling, Martin Fuchs, and Maria Paulin. Runoff conditions in the upper danube basin under an ensemble of climate change scenarios. *Journal of hydrology*, 424:264–277, 2012.

[64] Wouter JM Knoben, Jim E Freer, and Ross A Woods. Inherent benchmark or not? comparing nash–sutcliffe and kling–gupta efficiency scores. *Hydrology and Earth System Sciences*, 23(10):4323–4331, 2019.

[65] Raji Pushpalatha, Charles Perrin, Nicolas Le Moine, and Vazken Andréassian. A review of efficiency criteria suitable for evaluating low-flow simulations. *Journal of Hydrology*, 420:171–182, 2012.

[66] Daniel N Moriasi, Jeffrey G Arnold, Michael W Van Liew, Ronald L Bingner, R Daren Harmel, and Tamie L Veith. Model evaluation guidelines for systematic quantification of accuracy in watershed simulations. *Transactions of the ASABE*, 50(3):885–900, 2007.

[67] Toreti A, Bavera D, Acosta Navarro J, Arias-Muoz C, Avanzi F, Marinho Ferreira Barbosa P, De Jager A, Di Ciollo C, Ferraris L, Fioravanti G, Gabellani S, Grimaldi S, Hrast Essenfelder A, Isabellon M, Jonas T, Maetens W, Magni D, Masante D, Mazzeschi M, Mccormick N, Meroni M, Rossi L, Salamon P, and Spinoni J. Drought in europe march 2023. (KJ-NA-31-448-EN-N (online)), 2023.

[68] Alberto Montanari, Hung Nguyen, Sara Rubinetti, Serena Ceola, Stefano Galelli, Angelo Rubino, and Davide Zanchettin. Why the 2022 po river drought is the worst in the past two centuries. *Science Advances*, 9(32):eadg8304, 2023.

[69] Gemma Coxon, J Freer, Ida K Westerberg, Thorsten Wagener, Ross Woods, and PJ Smith. A novel framework for discharge uncertainty quantification applied to 500 uk gauging stations. *Water resources research*, 51(7):5531–5546, 2015.

[70] Manuela I Brunner, Anne F Van Loon, and Kerstin Stahl. Moderate and severe hydrological droughts in europe differ in their hydrometeorological drivers. *Water Resources Research*, 58(10):e2022WR032871, 2022.

[71] Christian Massari, Francesco Avanzi, Giulia Bruno, Simone Gabellani, Daniele Penna, and Stefania Camici. Evaporation enhancement drives the european water-budget deficit during multi-year droughts. *Hydrology and Earth System Sciences*, 26(6):1527–1543, 2022.

[72] Yuting Yang, Michael L Roderick, Hui Guo, Diego G Miralles, Lu Zhang, Simone Fatichi, Xiangzhong Luo, Yongqiang Zhang, Tim R McVicar, Zhuoyi Tu, et al. Evapotranspiration on a greening earth. *Nature Reviews Earth & Environment*, pages 1–16, 2023.

[73] Moctar Dembélé, Markus Hrachowitz, Hubert HG Savenije, Grégoire Mariéthoz, and Bettina Schaefli. Improving the predictive skill of a distributed hydrological model by calibration on spatial patterns with multiple satellite data sets. *Water resources research*, 56(1):e2019WR026085, 2020.

[74] Doris Duethmann, Aaron Smith, Chris Soulsby, Lukas Kleine, Wolfgang Wagner, Sebastian Hahn, and Dörthe Tetzlaff. Evaluating satellite-derived soil moisture data for improving the internal consistency of process-based ecohydrological modelling. *Journal of Hydrology*, 614:128462, 2022.

[75] Oldrich Rakovec, Rohini Kumar, Sabine Attinger, and Luis Samaniego. Improving the realism of hydrologic model functioning through multivariate parameter estimation. *Water Resources Research*, 52(10):7779–7792, 2016.

[76] G Hartmann and A Bárdossy. Investigation of the transferability of hydrological models and a method to improve model calibration. *Advances in Geosciences*, 5:83–87, 2005.

[77] Ponnambalam Rameshwaran, Victoria A Bell, Matthew J Brown, Helen N Davies, Alison L Kay, Alison C Rudd, and Catherine Sefton. Use of abstraction and discharge data to improve the performance of a national-scale hydrological model. *Water Resources Research*, 58(1):e2021WR029787, 2022.

[78] Jacopo Dari, Pere Quintana-Seguí, Renato Morbidelli, Carla Saltalippi, Alessia Flammini, Elena Giugliarelli, María José Escorihuela, Vivien Stefan, and Luca Brocca. Irrigation estimates from space: Implementation of different approaches to model the evapotranspiration contribution within a soil-moisture-based inversion algorithm. *Agricultural Water Management*, 265:107537, 2022.

[79] C Wade Ross, Lara Prihodko, Julius Anchang, Sanath Kumar, Wenjie Ji, and Niall P Hanan. Hysogs250m, global gridded hydrologic soil groups for curve-number-based runoff modeling. *Scientific data*, 5(1):1–9, 2018.

[80] Tomislav Hengl, Jorge Mendes de Jesus, Gerard BM Heuvelink, Maria Ruiperez Gonzalez, Milan Kilibarda, Aleksandar Blagotić, Wei Shangguan, Marvin N Wright, Xiaoyuan Geng, Bernhard Bauer-Marschallinger, et al. Soilgrids250m: Global gridded soil information based on machine learning. *PLoS one*, 12(2):e0169748, 2017.

[81] Wouter Dorigo, Wolfgang Wagner, Clement Albergel, Franziska Albrecht, Gianpaolo Balsamo, Luca Brocca, Daniel Chung, Martin Ertl, Matthias Forkel, Alexander Gruber, et al. Esa cci soil moisture for improved earth system understanding: State-of-the art and future directions. *Remote Sensing of Environment*, 203:185–215, 2017.

[82] Randolph Glacier Inventory – A Dataset of Global Glacier Outlines: Version 6.0: Technical Report, Global Land Ice Measurements from Space, Colorado, USA. Digital Media. DOI: https://doi.org/10.7265/N5-RGI-60. Technical report, RGI Consortium, 2017.